For Official Use **ENV/CHEM/NANO(2015)30/ADD5**

Organisation de Coopération et de Développement Économiques
Organisation for Economic Co-operation and Development **29-Oct-2015**

English - Or. English

ENVIRONMENT DIRECTORATE
CHEMICALS COMMITTEE

Working Party on Manufactured Nanomaterials

Draft "Nano-SIAR": Zinc Oxide

15th Meeting of the Working Party on Manufactured Nanomaterials
4-6 November 2015
OECD Conference Centre, Paris, France

Mrs. Mar Gonzalez. Tel. +33 1 45 24 76 96; Email: mar.gonzalez@oecd.org

JT03385395

Complete document available on OLIS in its original format

ENV/CHEM/NANO(2015)30/ADD5
For Official Use

English - Or. English

Preamble

This draft SIAR document has been provided in late October. The original version includes several comments and has not been assessed yet. One of the main information highlighted in the comments is that this SIAR document contains data related to non-OECD material. The testing methods as well as the material used have to be evaluated. This document can be used for discussion during the WPMN 15th and the data cannot be used for risk assessment or for regulation purposes. A full version with the comments is available in the OECD password protected site.

TABLE OF CONTENTS

DRAFT

Nano Zinc Oxide
(CAS 1314-13-4)
Assessment Report
Prepared for the OECD WPMN

Date: 25 August 2015

Abbreviation list

BET	Brunauer–Emmett–Teller
CPC	Condensation Particle Counters
CPS	centrifugal sedimentation
CSIRO	Commonwealth Scientific and Industrial Research Organisation
DI water	deionized water
DLS	Dynamic Light Scattering
DMA	Differential Mobility Analyzer
DTA	Differential Thermal Analysis
ECHA	European Chemical Agency
FBAG	Fluidised Bed Aerosol Generator
IEP	isoelectrical point
NM	Nanomaterial
NPL	National Physical Laboratory
OECD	Organisation for Economic Co-operation and Development
PROSPEcT:	Ecotoxicology Test Protocols for Representative Nanomaterials in Support of the OECD Sponsorship Programme
SEM	Scanning Electron Microscope
SMPS	Scanning Mobility Particle Sizer
TEM	Transmission electron microscopy
TG	Thermogravimetric thermal analyser
TOF-SIMS	Time of Flight Secondary Ion Mass Spectrometry
XPS	X-ray photoelectron spectroscopy
XRD	X-ray diffraction

Physical and Chemical Properties of Zinc Oxide (ZnO) Nanomaterials (NM)

Name and other identifiers of the substance

CAS Number:	1314-13-2
IUPAC Name:	oxozinc
Molecular Formula:	OZn
Structural Formula:	Zn=O
Molecular Weight:	81.4084 g/mol
Synonyms:	zinc oxide

Nano-material (NM) code	Type of material	Product name	Surface coating	Supplier
NM-110	Zinc Oxide, uncoated	Z-cote ®	None	BASF
NM-111	Zinc Oxide, coated	Z-cote HP 1	triethoxycaprylylsilane (2%)	BASF
NM-112	Zinc Oxide, uncoated	Nanosun™	None	Micronisers
NM-113*	Zinc Oxide, uncoated	Micron ZnO	None	Sigma Aldrich

*NM-113 = bulk material, not nano sized

Information requirements for physical and chemical parameter

In general, the nano specific physical and chemical properties were evaluated and reported in the following sections.

However, it is noteworthy to mention that the following endpoints were not investigated in this current evaluation report. It was assumed that results of the investigation of these endpoints will yield the same results compared to the bulk material. Please refer to the ECHA registration dossier of zinc oxide for the results of these endpoints:

- Melting point
- Boiling point

- Vapour pressure
- Water solubility
- Partition coefficient (octanol / water)
- Surface tension
- Flash point
- Auto flammability
- Explosiveness
- Oxidising properties
- Stability in organic solvents and identity of relevant degradation products
- Viscosity

Shape

The shape of the nanomaterials was investigated in studies by the Commonwealth Scientific and Industrial Research Organisation (CSIRO) in 2012 and by the Deakin University in 2012 using Transmission electron microscopy (TEM). According to the OECD guidance no suitable and validated procedure was available. Nevertheless, several guidelines (e.g. NIST, ISO 9276-6:2008) were available for the different parts of TEM method (e.g. sample preparation or sample splitting).

CSIRO, 2012 characterised the ZnO nanomaterials. All samples were glow discharged in nitrogen for 30 seconds to render them hydrophilic. Samples were dispersed by briefly sonicating a few milligram of the material in approximately 20 µl ethanol to form a milky dispersion. 5 µL of dispersion was applied to the freshly glow-discharged grids. After 2 min adsorption time, excess dispersion was wicked off using filter paper and the grids were air-dried for 15 min. Grids were examined using a Tecnai 12 TEM (FEI, Eindhoven, Netherlands) operating at 120 kV, and micrographs were recorded using an Olympus Megaview III CCD camera (Tokyo, Japan) running AnalySiS imaging software (Olympus) at a variety of magnifications chosen to show both the aggregation/agglomeration state of the samples (lower magnifications e.g. 6000x) as well as particle morphology (higher magnifications e.g. 100000x - 360000x). Typical TEM images of NM-110, NM-111, NM-112 and NM-113 are shown in Figure 1.

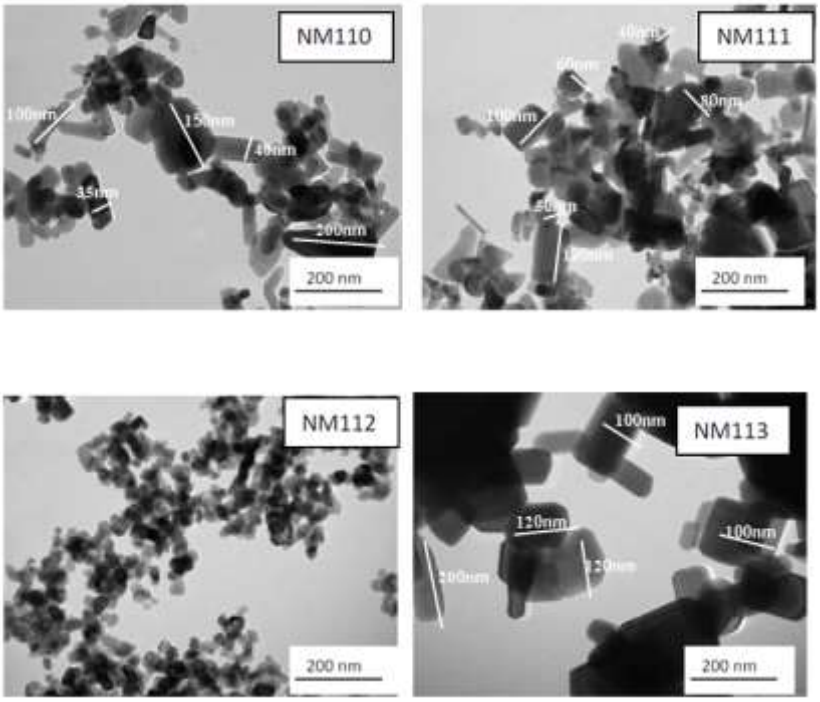

Figure 1: Typical TEM images of NM-110, NM-111, NM-112 and NM-113, taken at the same magnification of 200 nm

The four TEM images of the nanomaterials showing varied particle sizes and shapes in the different samples.

The TEM image of NM-110 indicated that the primary particles appeared polyhedral with variable morphology and size. Two main types of morphology could be distinguished:

- Particles with aspect ratio close to 1 (typically 20 – 250 nm size and very few particles of approx. 400 nm size) and hexagonal morphology
- Particles with aspect ratio 2 to 7.5 (50 – 350 nm) with cubic, tetragonal and orthorhombic morphologies.

The TEM image of NM-111 indicated that the primary particles appeared polyhedral and with variable morphology as observed in NM-110, but with different size distributions:

- Particles with aspect ratio near 1 (~90 % in the 20 – 200 nm range)
- Particles with aspect ratio 2 to 8.5 (~90 % in the 10 – 450 nm range)

The TEM image of NM-112 indicated that primary particles were near spherical (rather than polyhedral) with regular morphology and a relatively homogenous size distribution. Generally, particles had an aspect ratio close to 1, with sizes varying between 20 and 50 nm and appeared distinctly different to all the other samples (NM-110, NM-111 and NM-113).

- Particles with aspect ratio near 1 (typically in the 80 – 100 nm range)
- Particles with aspect ratio > 2 (typically in the 180 – > 200 nm range)

The TEM image of NM-113 showed that the sample was composed of polyhedral particles with sizes ranging generally between 100 to 200 nm, and with some larger agglomerates.

In addition a study conducted by the Deakin University, 2012 was also available. TEM specimen was prepared by evaporating a drop of the nanoparticle dispersion on a carbon-coated specimen grid. Grids were examined using a JEOL JEM-2100 TEM operating at 200 kV. No further details about the sample preparation and the method parameter were available.

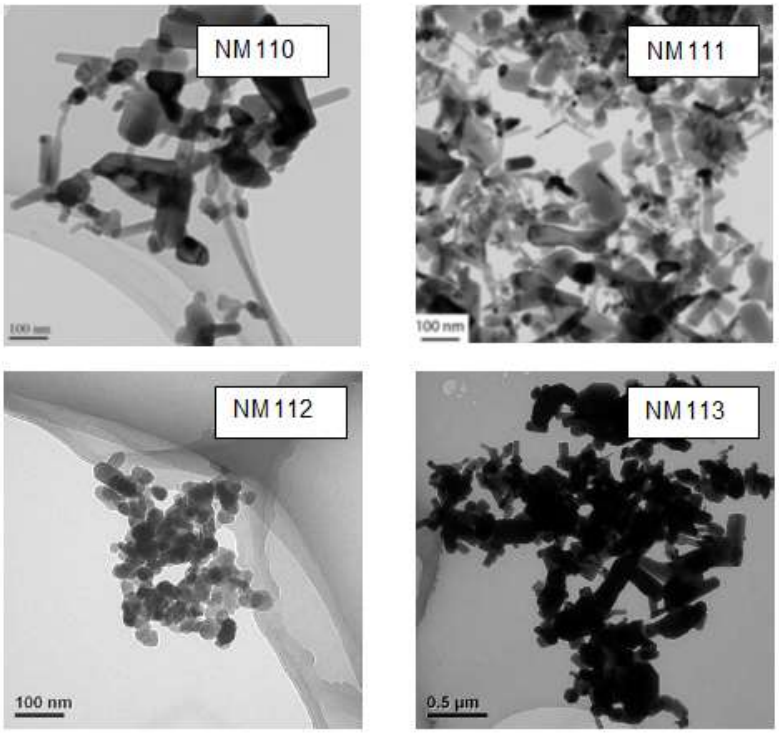

Figure 2: Typical TEM images of NM-110, NM-111, NM-112 at 100 nm and NM-113at 500 nm

The TEM image of NM-110 and NM-111 indicated wide distributions of shapes and sizes of primary particles. Furthermore the geometrical shapes indicated high crystallinity and low surface defects. The TEM image of NM-112 indicated near spherical shape of the primary particles and a high number of surface defects. The TEM image of NM-113 indicated geometrical shapes and large particle sizes (>100 nm in diameter).

The TEM images analyses in the course of the two studies yielded comparable results. The appearances of the particle as well as the morphology of the NM-110, NM-111 and NM-113 were comparable. The three NM were described as polyhedral with variable morphology and size. The NM-112 was determined to be

distinctly different to all the other samples. NM-112 was described to appears as near spherical and with the smallest particle size compared to the other 3 materials.

Dissolution / Dispersibility

A dissolution study conducted by CSIRO, 2012 in artificial soil solution of with ionic composition typical of that found in Australian soil porewater. The solution pH was buffered to 4, 7 or 9 throughout the dissolution study. The NM stock solution was added with 20 mL of artificial soil solution (final concentration of ~ 300 µg Zn/L) into 50 mL centrifuge tubes. The solution pH was maintained at 4, 7, or 9 using perchloric acid ($HClO_4$, 0.1 M) or sodium hydroxide (0.1 M) and buffered using 0.1 mM sodium acetate ($NaCH_3COO$), 0.1 mM 2-(N- morpholino)ethanesulfonic acid sodium salt (MES), or 0.1 mM sodium borate ($Na_2B_4O_7$ x 10 H_2O) solutions, respectively. The solutions were shaken on an end-over-end shaker for 0, 24h and 7d. At individual time periods, 2 mL of solution was removed and added into 1 kDa ultra filtration devices (UF). The UF devices were centrifuged at 4000 g for 15 min and total Zn concentrations in filtrates determined using inductively coupled plasma-mass spectrometry. The dissolution of NM in each pH solution and time period was expressed as a percentage of the total Zn added. The results are given in Table 1.

Table 1: Dissolution results

Time (day)	pH	NM-110 Dissolution (%)	NM-111 Dissolution (%)	NM-112 Dissolution (%)	NM-113 Dissolution (%)
0	4	91 ± 12	9.2 ± 1.4	89 ± 4	1.4 ± 0.1
1	4	96 ± 10	14.4 ± 1.1	81 ± 7	1.5 ± 0.02
7	4	105 ± 11	13.0 ± 2.3	82 ± 4	7.4 ± 0.6
0	7	53 ± 8	1.4 ± 2.8	62 ± 3	0.06 ± 0.001
1	7	67 ± 4	4.4 ± 3.8	60 ± 6	0.11 ± 0.01
7	7	58 ± 4	6.3 ± 4.6	65 ± 3	0.25 ± 0.08
0	9	< 2	7.2 ± 0.7	2.7 ± 1.0	0.009 ± 0.0045
1	9	< 2	11.8 ± 0.4	2.5 ± 0.5	0.007 ± 0.0001
7	9	< 2	11.4 ± 0.4	2.8 ± 0.6	0.007 ± 0.0001

In addition the National Physical Laboratory (NPL), 2010 investigated the dispersion of NM-110, NM-112 and NM-113 in an ecotoxicology relevant media (fish medium, daphnia medium and seawater). Deionised water was employed as the corresponding media control and was used to prepare all aqueous solutions and suspensions. Zinc ions were measured using Cole-Palmer® Colorimetric Test Kits (Cole Palmer, UK). The colorimetric measurement was used to evaluate the nanomaterials when dispersed in different media over time of 21 days; the extracted supernatant from the dispersions were obtained prior to performing the colorimetric tests. The dispersions were stored in a refrigerator after day 2 in order to prevent degradation of the sample e.g. minimising bacterial growth.

It was shown that dissolution rates were fastest, when the NMs were dispersed in deionized water, with NM-110 dissolving fastest and NM-112 dissolving slowest. Deionized water yielded the most stable dispersions and this increase in stability will result in less aggregation/agglomeration (and subsequent sedimentation) in the dispersion. The total surface area was greater when the particles were dispersed in deionized when compared to corresponding ecotox media. Thus, an increase in surface area means that the ion dissolution rate will also increase. An apparent decrease in zinc concentrations from Day 6 to Day 9, for all zinc oxide NMs was observed. This effect may be indicative of the dissolution-precipitation process occurring during this time. Out of all the ecotox media, fish medium had highest dissolution rate followed by daphnia and then seawater. Dispersing nanomaterials in such ecotox media would mean less stable dispersion and this subsequently equates to the reduced surface area concentrations and thus a lower dissolution rate.

Furthermore NPL, 2010 investigated the dissolution of NM-110, NM-112, NM-113 in different media (deionized water, fish medium, daphnia medium and seawater) using inductively coupled plasma mass spectrometry (ICP-MS). Dispersion was performed in accordance to the recommended PROSPEcT protocol. A concentration of 50 mg/L was made up for each sample; a total volume of 1 L was made up and stored in clean media (1 L) bottles at room temperature. After day 2, the bottles were stored in the fridge. Several extractions from the 1 L sample were made over a period of 22 days. The extracted sample (~ 50 mL) was then subjected to a three-step process in order to remove particles and to extract the resultant supernatant. The results are given in Table 2.

Table 2: ICP-MS test results

Media	**Day**	**Zinc concentration of the supernatant extracted (ng/g)**		
		NM-110	NM-112	NM-113
deionized water	2	2536	764	1864
	6	3360	1741	3436
	9	3130	1490	2813
	14	3772	1808	3005
	22	5030	1607	6007
Fish	2	2216	1198	1780
	6	2192	1632	2442
	9	3028	1744	2420
	14	2697	1676	2961
	22	3036	1954	3239
Daphnia	2	1454	1158	1465
	6	N/A	1458	1644
	9	1014	1731	1515
	14	1588	1052	2193

Media	Day	Zinc concentration of the supernatant extracted (ng/g)		
	22	2037	1402	2611
Seawater	2	681	241	531
	6	736	371	466
	9	773	439	605
	14	972	420	1089
	22	1155	359	1051

Dissolution rates were fastest when the NMs were dispersed in deionized water, with NM-110 dissolving the fastest and NM-112 dissolving the slowest. Deionized water yielded the most stable dispersions and this increase in stability will mean less aggregation/agglomeration (and subsequent sedimentation) in the dispersion. Out of all the ecotox media, fish medium had the largest dissolution rate followed by daphnia and then seawater. Dispersing NMs in such ecotox media would mean less stable dispersion and this subsequently equates to the reduced surface area concentrations and thus a lower dissolution rate.

A publication by Rogers et al., 2010, was available. The dissolution of NM-110 in synthetic softwater medium without EDTA and buffered at pH 7.5 ± 0.1 with 2 mM piperazine-N,N'-bis(ethanesulfonic acid) was determined using the equilibrium dialysis technique described by Franklin et al., 2007. The dissolution of NM-110 was determined to be 6.77 ± 0.12 mg/L at pH = 7.5 in US EPA medium. Due to the different test procedure, conditions and the lack of data from the other three nanomaterials, this result was regarded as less relevant.

Particle size distribution

Several studies using different analytical techniques were available for particle size of the investigated nanomaterials.

The National Physical Laboratory (NPL), 2010 investigated the particle size distribution of the 4 test items. In accordance with the ECHA guidance size distribution was investigated using multiple techniques. According to the OECD guidance no single suitable and validated procedure is currently available. Therefore different analytical measures using Transmission Electron Microscopy (TEM), Scanning Electron Microscopy (SEM), Dynamic Light Scattering (DLS), Scanning Mobility Particle Sizer (SMPS), centrifugal sedimentation method (CPS) and X-ray diffraction (XRD) were conducted.

NPL, 2010 investigated the particle size of the test items NM-110, NM-112 and NM-113 using TEM. Therefore a nanomaterial sample dispersion of 50 mg/L was made in accordance to the OECD recommended protocol for sample dispersion. The dispersion was allowed to settle out in order to remove the larger particles naturally as it sediments by gravity. The purpose of this sedimentation was to remove large micron size particles. On day 2, there was clear visible evidence of sedimentation events of the larger micron size particles having taken place. Two microliter aliquots were extracted from the top layer (an opaque but slightly transparent layer). The sample was placed on TEM grids and allowed to air dry for 10

minutes; grids are formvar/carbon on 400 meshes copper. Grids were used as supplied with no further modification. All images were recorded using a Hitachi 2300 A instrument operated at 200 kV. An adequate magnification was chosen for image acquisition e.g. for the estimation of primary particle mean diameter. TEM micrographs were analysed by manually tracing contours of primary particles on to a transparency sheet. The transparency sheet was scanned for further image analysis using ImageJ software, which automatically calculated particle diameter dimensions. Furthermore an extremely small area of the sample could be analysed, which might not be representative enough for the whole sample. The comparatively small share of evaluated particles results in limited statistical precision. The mean primary particle size was quoted with the corresponding standard deviation which represents the broadness of the size distribution.

A histogram of the analysis of NM-110 is presented in Figure 3. Based on the measurements of 77 particles the mean particle size of the NM-110 was determined to be 75.4 ± 58.4 nm.

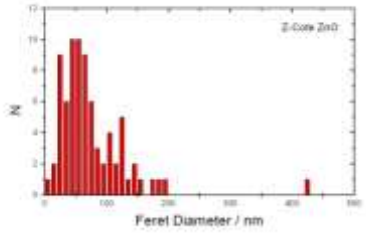

Figure 3: Particle size distribution of NM-110

A histogram of the analysis of NM-111 is presented in Figure 4. Based on the measurements of 312 particles the mean particle size of the NM-111 was determined to be 30.5 ± 13.8 nm.

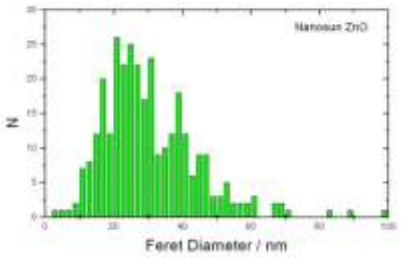

Figure 4: Particle size distribution of NM-111

A histogram of the analysis is presented in Figure 5. Based on the measurements of 87 particles the mean particle size of NM-113 was determined to be 165.2 ± 90.4 nm.

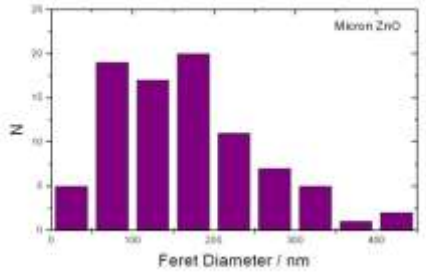

Figure 5: Particle size distribution of NM-113

NPL, 2010 investigated the particle size of the test items NM-110, NM-112 and NM-113 using DLS. Hydrodynamic size (z-average mean) measurements were obtained using a Zetasizer Nano ZS (Malvern Instruments, UK) equipped with a 633 nm laser. A reference standard (polystyrene, latex bead, nominal size of 100 nm, NIST traceable) was used to qualify the performance of the instrument. Sample analysis involved filling of a disposable capillary cell (DTS1060, Malvern). Prior to their use, these cells were thoroughly cleaned with ethanol and de-ionised water, as recommended by the instrument vendor. Individual cell was then filled with the appropriate sample and flushed before re-filling; measurement was carried out on the second filling. Malvern Instrument's Dispersion Technology software (Version 4.0) was used for data analysis. For particle size it was the z average diameter (the mean hydrodynamic diameter) that was reported. The protocol for sample preparation was described by Tantra, R., Jing, S. and Gohil, D.in Technical issues surrounding the preparation, characterisation and testing of nanoparticles for ecotoxicological studies, in Environmental Toxicology 3, V.B. Popov, C.A., Editor. 2010, WIT Press p. 165-176.

The mean particle size of three distributions was determined to be 275 nm for NM-110, 253 nm for NM-112 and 508 nm for NM-113 respectively.

NPL, 2010 used XRD to determine the particle size of the nanomaterials. XRD traces were obtained using a Siemens D5000 diffractometer. This consisted of a theta-theta goniometer and an NPL specimen stage. The X-ray source used for these measurements was the Cu- K_{alpha} X-ray (40 kV, 30 mA) filtered using a Ni filter that removed the Cu- $K_{ß}$ component of the X-ray. The X-ray optics consisted of a 0.6 mm anti-scatter slit, a 1 mm collimation slit and a 1 mm detector slit. The diffraction measurement was conducted using coupled theta-theta drives in standard Bragg-Brentano geometry. The data was collected over a 2-theta range of 5 to 150° using a step size of 0.010° and a count time of 1.5 s per step. Prior to the measurement the X-ray beam was aligned by placing the X-ray source and the detector in line and passing the X-ray beam through a glass slit, the direct beam was attenuated using copper foil placed in front of the detector. Having aligned the two drives and the stage height a standard reference material (corundum) was used to check the alignment over a range of 2-theta values. Particle size was determined using Scherre's equation. The results are given in Table 3.

Table 3: Numerical results for the XRD analysis

Sample	Particle size (nm)
NM-110	41.5
NM-111	33.8
NM-112	24.1
NM-113	41.5

NPL, 2010 determined particle size distribution of Aerosolised nanomaterials by SMPS consisting of a Differential Mobility Analyser (DMA) and Condensation Particle Counters (CPC) system. The DMA within the SMPS was calibrated using reference material polystyrene latex beads from NIST. TSI Fluidised Bed Aerosol Generator (FBAG) was used to produce an aerosol from the dry powder sample. After introduction of the nanomaterial into the FBAG, the aerosol generated was allowed to stabilise for a day prior to sending the aerosol to an SMPS. The CPC within the SMPS setup were calibrated according to NPL's UKAS accredited (ISO 17025) procedure, using an internally calibrated Faraday Cup Electrometer and soot generator (model CAST 2). The SMPS was set to record at 4 minute intervals; at least 6 SMPS scans of 200 seconds each were used for analysis. The data was processed using TSI Aerosol Instrument Management (AIM) software, in which the mean size distribution from the stable time segment was estimated. The size distribution was also analysed using an in-house curvefitting program (as implemented in a recent SMPS intercomparison at METAS).

In order to estimate the effective mean, a lognormal was fitted to the distribution and the geometric mean was estimated. Geometric Mean particle sizes of the different aerosolised powders as measured by SMPS are given in Table 4.

Table 4: Geometric Mean particle size of the different aerosolised nanomaterials

Sample	Geometric Mean Particle Size (nm)	Geometric Standard Deviation of log-normal
NM-110	289	1.68
NM-111	400	1.57
NM-112	269	1.80
NM-113	300	1.63

NPL, 2010 determined the particle size distribution by SEM. SEM images were obtained using a Supra 40 field emission scanning electron microscope from Carl Zeiss (Welwyn Garden City, Hertfordshire, UK), in which the optimal spatial resolution of the microscope was a few nanometres. For analysis of the "as received" nanoparticle powder, a sample of the powder was sprinkled over a SEM carbon adhesive disc; one side of the carbon disc was placed securely on a metal stub, whilst the other side was exposed to the nanoparticle powder. Excess powder was removed by gently tapping the stub on its side until a light coating of powder on the surface became apparent. An adequate magnification was chosen for image

acquisition e.g. for the estimation of primary particle mean diameter. The shape and limits of the primary particles should become apparent. SEM micrographs were analysed manually; this was done by manually tracing contours of primary particles on to a transparency sheet. The transparency sheet was scanned for further image analysis using ImageJ software, which automatically calculated particle.

The mean Feret diameter was determined to be 151 nm for NM-110, 140.8 nm for NM-111, 42.5 nm for NM-112 and 891.8 nm for NM-113 respectively.
Furthermore the results of the homogeneity study were reported. The total weighted mean for NM-110 was determined to be 120 nm and the total weighted mean for NM-111 was determined to be 120 nm respectively. Results suggest that there is no significant difference in the mean primary particle size (and corresponding SD) between the two types of NMs and no real differentiation in the mean primary particle size between the vials in one type of sample.

CSIRO, 2012 investigated the particle size distribution of the 4 nanomaterials. The particle size was determined using XRD, TEM and Brunauer–Emmett–Teller (BET) surface area measurements. Two XRD methods were used to estimate average crystallite size based on XRD results. The $D_{S\text{-}XRD}$ was calculated using Scherrer's formula and $D_{R\text{-}XRD}$ was calculated using DIFFRACplus TOPAS 4.2 through Rietveld refinement of the diffraction data.

For TEM measurements two methods were used to estimate average particle size based on TEM results. Both Feret's diameter and the equivalent circular diameter were determined by measuring 100 individual particles in TEM images. The BET measurements were performed under the assumption that that all particles in the sample have a spherical shape, a smooth surface and are the same size. The average equivalent particle size (DSA BET) was calculated from measurements of BET surface area.

Table 5: Results of the Particle size determination

Sample	$D_{R\text{-}XRD}$ (nm)	$D_{S\text{-}XRD}$ (nm)	$D_{Feret\ TEM}$ (nm)	$D_{circ\ TEM}$ (nm)	$D_{SA\ BET}$ (nm)	Average of all methods (nm)
NM-110	113	41	70 ± 46	52 ± 33	74	77.5 ± 18
NM-111	83	34	82 ± 45	60 ± 33	76	75.2 ± 7.6
NM-112	43	25	30 ± 9	25 ± 7	37	33.75 ± 6.2
NM-113	200	42	143 ± 47	113 ± 45	143	149.7 ± 25.0

All methods indicate that the particle sizes are in the same size range. Based on the average values from all methods, the particle size was determined to be ~34 nm for NM-112, 78 nm for NM-110, 75 nm for NM-111 and 150 nm for NM-113. The particles size determined by different methods were generally in the order of $D_{R\text{-}XRD} > D_{SA\ BET} \sim D_{Feret\ TEM} > D_{Circ\ TEM} > D_{S\text{-}XRD.}$ $D_{S\text{-}XRD}$ was smallest because Scherrer's formula ignores the contributions of width broadening due to strain and instrument effects. If these contributions are non-zero, the crystallite sizes could be larger than those predicted by the Scherrer's formula, as revealed by $D_{R\text{-}XRD}$. The real states of particles can be described as singlets, agglomerates or

aggregates. Agglomerates are primary particles held by weak Van der Waals force that can be overcome if sufficient energy is provided. Aggregates are primary particles held together by strong chemical bonds that cannot be separated by conventional methods. $D_{Feret\text{-}TEM}$ provides the most reliable assessment of aggregate size, because aggregates are not broken up by ultrasonication during sample preparation whereas agglomerates can be. $D_{Circ\text{-}TEM}$ provides a smaller value than $D_{Feret\text{-}TEM}$ since this method treats all particles as spheres; it is not the most suitable method for analysing samples containing particles with a broad or multimodal size distribution. $D_{SA\text{-}BET}$ was calculated from measurements of specific surface area and assumed that all particles are non-porous and have the same spherical shape and size.

NPL, 2010 investigated the particle size distribution using CPS Disc Centrifuge. Analysis was run against a calibration standard, NIST traceable standard, PVC 0.377 micron. The results are presented in Table 6.

Table 6: D_{10}, D_{50}, D_{90} values from the averaged centrifugal sedimentation measurements

Sample	deionized water (nm)	Fish medium (nm)	Seawater (nm)	Daphnia (nm)
NM-110	D_{90} 286 ± 2 D_{50} 82.8 ± 1.9 D_{10} 107.3 ± 1.7	D_{90} 400 ± 30 D_{50} 270 ± 20 D_{10} 130 ± 30	D_{90} 417 ± 12 D_{50} 301 ± 8 D_{10} 193 ± 7	D_{90} 410 ± 20 D_{50} 285 ± 16 D_{10} 140 ± 30
NM-112	D_{90} 720 ± 30 D_{50} 40.1 ± 0.7 D_{10} 64.6 ± 0.6	D_{90} 1000 ± 200 D_{50} 190 ± 17 D_{10} 93 ± 4	D_{90} 1180 ± 20 D_{50} 330 ± 70 D_{10} 130 ± 50	D_{90} 100 ± 200 D_{50} 400 ± 200 D_{10} 100 ± 50
NM-113	D_{90} 870 ± 60 D_{50} 572 ± 19 D_{10} 306 ± 7	D_{90} 890 ± 40 D_{50} 606 ± 12 D_{10} 336 ± 8	D_{90} 930 ± 50 D_{50} 639 ± 15 D_{10} 399 ± 14	D_{90} 930 ± 20 D_{50} 612 ± 3 D_{10} 332 ± 6

[The results are partly contradictory as D_{50} portion is sometimes lower/higher than D_{10} and/or D_{90}.The results were corrected as D10 and D90 values were reversed in the original data].

There are some discrepancies in the provided data of the study. The result of NM-112 in deionized water and Daphnia media and NM-110 in deionized water seems to be erroneous as the trend of the particle size distribution is not consistent. Nevertheless, the results show that the largest mean particle size exists when the NMs are dispersed in seawater; this is reflected on the particle mean size as well as the corresponding D_{90} values. The equivalent spherical mean particle diameter was determined to be for NM-110 193 ± 3 nm in DI water, 290 ± 20 nm in fish medium 309 ± 10 nm in seawater and 296 ± 16 nm in daphnia media respectively. The equivalent spherical mean particle diameter was determined to be for NM-112 277 ± 7 nm in DI water, 390 ± 70 nm in fish medium 510 ± 40 nm in seawater and 500 ±200 nm in daphnia media respectively. The equivalent spherical mean particle diameter was determined to be for NM-131 590 ±30 nm in DI water, 620 ± 20 nm in fish medium 660 ± 20 nm in seawater and 631 ± 5 nm in daphnia media respectively. The results show that the largest mean particle size exists when the NMs are dispersed in seawater; this is reflected on the particle mean size as well as the corresponding D90 values. Results also show that the smallest particle size exists when the NMs are dispersed in deionized water. This suggests that larger agglomerates exist in the ecotox media, i.e. largest agglomerates found in seawater.

NPL, 2010 determined particle size distribution by SEM. SEM images were obtained using a Supra 40 field emission scanning electron microscope from Carl Zeiss (Welwyn Garden City, Hertfordshire, UK), in which the optimal spatial resolution of the microscope was a few nanometres. For analysis of the "as received" nanoparticle powder, a sample of the powder was sprinkled over a SEM carbon adhesive disc; one side of the carbon disc was placed securely on a metal stub, whilst the other side was exposed to the nanoparticle powder. Excess powder was removed by gently tapping the stub on its side until a light coating of powder on the surface became apparent. An adequate magnification was chosen for image acquisition e.g. for the estimation of primary particle mean diameter. The shape and limits of the primary particles should become apparent. SEM micrographs were analysed manually. This was done by manually tracing contours of primary particles on to a transparency sheet. The transparency sheet was scanned for further image analysis using ImageJ software, which automatically calculated particle. The mean Feret diameter was determined to be 151 nm for NM-110, 140.8 nm for NM-111, 42.5 nm for NM-112 and 891.8 nm for NM-113 respectively.

NPL, 2010 investigated the particle size distribution of the NM-110 by SEM. SEM images were obtained using a Supra 40 field emission scanning electron microscope from Carl Zeiss in which the optimal spatial resolution of the microscope was a few nanometres. In-lens detector images were acquired at an accelerating voltage of 15 kV, a working distance of ≈ 3 mm, and a tilt angle 0°. SEM instrument was calibrated using a SIRA grid calibration set (SIRA, Chislehurst, Kent, UK). These are metal replicas of cross ruled gratings of area of 60 mm2 with 19.7 lines/mm for low magnification and 2160 lines/mm for high magnification calibrations, accurate to 0.2 %. For analysis of the "as received" nanoparticle powder, a sample of the powder was sprinkled over a SEM carbon adhesive disc; one side of the carbon disc was placed securely on a metal stub, whilst the other side was exposed to the nanoparticle powder. Excess powder was removed by gently tapping the stub on its side until a light coating of powder on the surface became apparent. An adequate magnification was chosen for image acquisition e.g. for the estimation of primary particle mean diameter. The shape and limits of the primary particles should become apparent. The SEM images were opened in ImageJ (a free image analysis program produced and distributed by the National Institute of Health, US) installed on a Tablet PC (DELL XT1), and for each image at least 20 distinct particles identified, to measure at least 100 particles per replicate. The particles chosen were an array of sizes to accurately represent the variety in the sample. Using the Pencil Tool (pencil width 2 pixels, colour black) the outlines of these particles were drawn using the supplied digital 'pen'. The image was calibrated with reference to the scale marking on the image. Then the threshold level adjusted so that only the particle outlines were highlighted. The particles were then measured using the Analyze Particles tool, which produced a results table of various measurements of the particles. This process was repeated for each image of the particular replicate (seven in total – giving a minimum of 140 particles identified. Feret's diameter – also called the "maximum calliper length", i.e. the longest distance between any two points along the selection boundary - was recorded and the scientific graphing and analysis software, SciDAVis, where a histogram (bin size 2) was plotted, showing the particle size distribution of the replicate. The entire process was repeated for each replicate (r1, r2, r3) for all six sub-samples of both the ZnO and ZnO-HP1 samples.

From the SEM image a broad range of particle sizes were seen from small (20-50 nm) circular or spherical particles, to much larger (>100 nm) rod shaped particles. Overall, the particle size distributions between

replicates per sub-sample are very similar, only differing by an average range of 14.6nm for the ZnO-HP1 sample and 8.4nm for the ZnO sample. An exception however, is the difference in the replicates of sub-sample 0830 for NM-100.The mean particle size for NM-110 is in the range 70-80nm, and for the ZnO sample the range 100-111nm. Except for sub-sample 1455 which is 93.3nm, larger than that of the other sub-samples for NM-110 and for ZnO, sub-sample 0599 at 90.3nm has a comparatively small mean particle size.

It was shown that the analysed particle size is depending on the applied method as well as the use of representative sample volume and medium. All applied methods are recommended by the ECHA guidance but the provided reports do not completely fulfil the current requirements for data evaluation and reporting. Furthermore no data about the particle size distribution of the powder nanomaterials was provided. Therefore a reliable evaluation of the provided data and classification was not possible.

However, the data used as weight-of-evidence in principle shows, that the same analytical method achieved comparable results. The XRD analysis conducted by NPL, 2010 and by CSIRO, 2012 are in good consistence. Furthermore, based on the available data the basic assumption (NM-113 as "bulk material" has the largest particle size) could be confirmed. Throughout all measurements NM-112 was determined to have the smallest particle size compared to the other 3 NMs. The results of the different measurements of NM-110 and NM-111 samples show that these 2 NMs have a comparable particle size. This general trend was also observed for the endpoints density and surface area, which are directly linked with the particle size.

Thermal stability

CSIRO, 2012 determined the thermal properties of the different nanomaterials using a Setaram Evolution Differential Thermal Analysis / Thermogravimetric (DTA/TG) thermal analyser with a carrier gas of air or argon, and using a heating ramp rate of 20°C/min to a maximum temperature of 1100°C. Volatile species were simultaneously analysed by mass spectrometry; species of interest were those with atomic mass units of 2, 12, 16, 17, 18, 28, 44, 48, and 64.

Table 7: Per cent weight loss from ZnO samples heated under air or argon, as determined by DTA/TG

Sample	NM-110	NM-111	NM-112	NM-113
Weight loss under air	0.3 %	5.8 %	1.7 %	0.2 %
Weight loss under argon	0.3 %	4.1 %	1.3 %	0.6 %

All weight-losses were small (less than 6 %), indicating that little/no oxidation occurred up to 1100 °C. Slight differences in the degree of weight loss were observed between different samples; NM-110 and NM-113 were both very stable and exhibited minor losses (< 0.6 wt %) while losses from NM-111 and NM-112 were much higher (4-6 wt % and 1-2 wt % respectively). Mass spectrometry identified CO_2 and water when both NM-111 and NM-112 were heated in air, but not when NM-110 and NM-113 were heated in air. When heated in argon, traces of both CO_2 and water were identified in all samples. The 4-6 wt % loss by NM-111 suggests that the quantity of coating may be higher than the nominative 2 wt %. For

NM-111, the onset of coating decomposition occurred at similar temperatures in both air (328 °C) and argon (290 °C). However, NM-111 exhibited a much sharper and larger (5-7 times) exotherm in air compared with argon. These observations are consistent with thermal oxidation of the coating which occurs between 350 - 420 °C. Degradation via thermal depolymerization occurs at higher temperatures (420 - 480 °C). The respective exotherms of 311 J/g (air) and 40 J/g (argon) reflect the oxidative nature of the reaction for NM-111, and the larger amounts of CO_2 and water detected by mass spec (compared with uncoated samples NM-110, NM-112 and NM-113) confirm coating degradation. The fact that NM-112 is the only uncoated ZnO that exhibits CO_2 and water release at low temperatures combined with having the highest surface area suggests that it is more reactive in its adsorption behaviour and is more likely to be less stable in the longer term than its larger-sized counterparts.

In conclusion it was shown that the difference in thermal properties for the 4 nanomaterials is not linked with the material form (nano or bulk) but rather with coating.

Redox potential

NPL, 2010 investigated the redox potential measurements, using ORP probe electrode, of various ZnO dispersions (NM-100, NM-112 and NM-113), in various liquid media. NM-111 could not be investigated by this method as it was difficult to disperse. The redox potential ORP electrode was calibrated against Calibration Solution. This standard solution was also used to verify the performance of the electrode in the beginning and end of the study. Redox potential measurements were carried out on freshly dispersed NM in various media (deionized water, fish medium, daphnia medium and seawater). Dispersion of the individual nanomaterial in the appropriate liquid media was carried out in accordance to the protocol as recommended under PROSPECT/OECD (as part of the OECD guidelines).

Table 8: Redox potential of NM dispersion in various liquid media, the value quoted is relative to the standard hydrogen reference electrode; values quoted in mV.

Sample	NM-112	NM-113	NM-110
deionized water	398 mV	398 mV	396 mV
Fish media	424 mV	430 mV	427 mV
Daphnia media	415 mV	415 mV	422 mV
Seawater	380 mV	374 mV	379 mV

Furthermore NPL, 2010 determined the redox potential of NM-110 using cyclic voltammetric method. Results show two redox processes that are taking place, which was referred to as “Redox 1” and “Redox 2”. Each redox reaction consists of two half-reactions i.e. for oxidation and reduction reactions and these correspond to the oxidation peak and reduction peak in the C-V plot.

Furthermore it was indicated by the study director that the values should be treated with caution as:

a) Peaks were very broad, so numbers are only approximate.
b) Peak-peak separation was large, indicating that the processes were not fully reversible.

The reliability of the provided data could not be assigned. Therefore a final conclusion could not be made.

Agglomeration/aggregation

Two studies were available (CSIRO, 2012 and NPL, 2010) which investigated the agglomeration of the NMs as such and in different media.

CSIRO, 2012 investigated the agglomeration/aggregation of the nanomaterials. Therefore a Philips XL30 field emission SEM was used for this study. The optimal spatial resolution of the microscope was from 2-5 nm with varying accelerating voltage from 30 kV to 1 kV. Images of ZnO particles were acquired at an accelerating voltage of 5 kV, a working distance of ≈ 10 mm, and a tilt angle 0°. An SEM metal stub was covered with adhesive conducting tape and a small amount of "as received" ZnO powder (around 5 mg) was sprinkled over the tape. The surface of the powder sample was flattened with spatula. Excess powder was removed by gently tapping the stub on its side until a light coating of powder on the surface became apparent. The nanoparticles were thinly sputtered with iridium using a Polaron SC570 sputter coater. Sputtering was conducted under vacuum while passing gas was argon. The coating deposition time was 20 seconds at a plate current of 50 mA, giving a coating thickness of approximately 1 nm. Typical SEM pictures of four ZnO samples are presented in Figure 6. SEM images reveal that ZnO particles as powder without media were agglomerated.

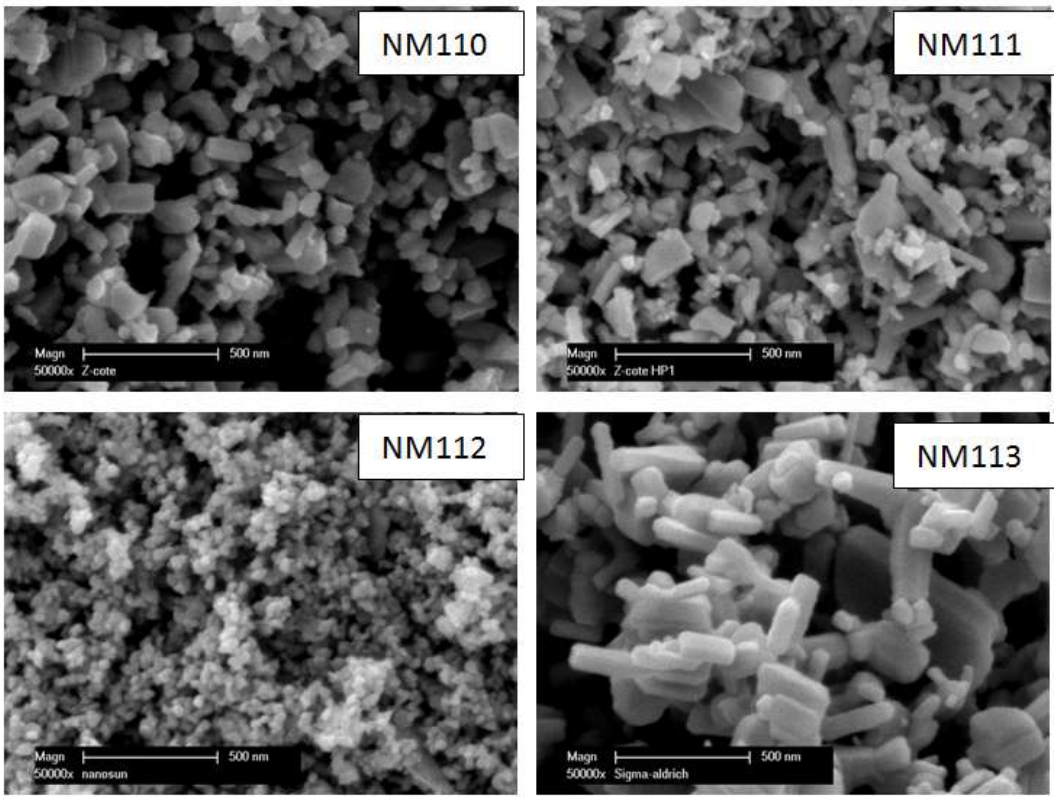

Figure 6: Typical SEM images of four ZnO samples, NM-110, NM-111, NM-112 and NM-113 at 500 nm.

The particle size was smallest for sample NM-112 and largest for NM-113, consistent with analyses of TEM images (please refer to section 0 and see Figure 1).

Furthermore CSIRO, 2012 determined the hydrodynamic size of the test items using Dynamic Light Scattering (DLS). DLS data were not obtained for sample NM-111, as its surface coating made it hydrophobic and the sample could not be dispersed readily in water. Measurements of hydrodynamic size were obtained using a Brookhaven particle size analyser 90Plus equipped with a 657 nm laser. Reference standards (Duke polystyrene latex, with a nominal size of 100 nm, and NIST RM8013 Au nanoparticles with a nominal size of 60 nm) were used to assess the performance of the instrument. 10 mg as received ZnO particles were added to a measuring cuvette containing 3 mL of deionised water. The cuvette was placed in an ultrasonic bath, ultrasonicated for 10 seconds and then shaken to ensure the particles were well dispersed before starting the dynamic light scattering measurements. Each size distribution curve and correlation function curve that was generated was based on 10 measurements. Experiments for each sample were performed in triplicate. The temperature was maintained at 25 °C. The cuvette was thoroughly washed with deionised water after each experiment. The measured hydrodynamic diameter for Duke polystyrene latex was 98 nm, and for NIST RM8013 Au nanoparticles was 61 nm.

The mean hydrodynamic sizes for NM-110, NM-112 and NM-113 were determined to be 338 nm, 444 nm and 466 nm respectively. These hydrodynamic diameters appeared to be independent of the primary particle sizes, suggesting that particles from the ZnO samples were aggregated /agglomerated when dispersed in deionized water.

SEM analysis indicated that the zinc oxide nanomaterials were highly agglomerated and aggregated. DLS indicated that in all cases the nanomaterials consisted of polydisperse distributions of particles. CPS disc centrifuge results indicated (please refer to section 0) that nanomaterials agglomeration was largest in seawater and smallest in deionized water indicating that larger agglomerates exist in ecotoxicology media.

Crystalline phase

CSIRO, 2012 investigated the crystallite phase of the nanomaterials. The crystalline phase was determined using a Bruker ASX-D8 XRD using Cu K (alpha) radiation. The operation current and voltage was 40 mA and 40 kV respectively. The scan ranged from 5° to 85° with a step size of 0.02° and a scan speed of 0.40 second/step. The aperture slit size directing the x-ray source was 0.2 mm.

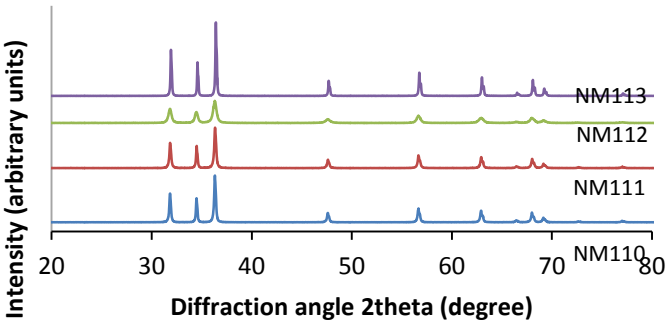

Figure 7: XRD patterns for NM-110, NM-111, NM-112 and NM-113

XRD patterns of the four ZnO samples are shown in Figure 7 and indicated that all ZnO nanomaterial samples were in a hexagonal wurtzite zincite crystalline phase.

Furthermore the Australia Deakin University, 2012 investigated the crystalline phase of the test items. The crystallite phase was determined using an X'Pert Pro MRD X-Ray Diffractometer (XRD) using Cu $K_{(alpha)}$ radiation. The operation current and voltage was 40 mA and 40 kV respectively. The scan ranged from 10° to 80° with a step size of 0.02° and a scan speed of 0.50 second/step. The aperture slit size directing the x-ray source was 200 nm.

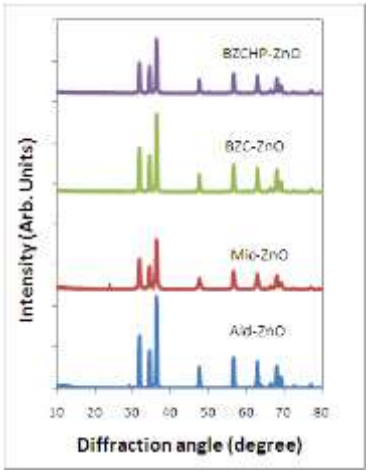

Figure 8: XRD patterns for NM-110, NM-111, NM-112 and NM-113

XRD patterns of the four ZnO samples are shown in Figure 8 and indicated that all ZnO nanomaterial samples were in a hexagonal wurtzite zincite crystalline phase.

In two independent studies using different apparatuses, it was concluded that all ZnO nanomaterial samples were in a hexagonal wurtzite zincite crystalline phase. Therefore, it was concluded that the crystalline phase of zinc oxide is independent from the material form (bulk or nano).

Crystallite size

NPL, 2011, investigated the crystallite size of the nanomaterials. To characterise the zinc oxide (ZnO) nanomaterials XRD traces were obtained using a Siemens D5000 diffractometer. Crystallite size was determined using Scherrer equation. The pattern matches were performed using this software linked to the ICDD (International Centre for Diffraction Data) PDF (Powder Diffraction File) database 2005). The crystallite sizes determined from the XRD patterns are given in Table 9.

Table 9: Crystallite size as determined from the XRD patterns using the Scherrer equation

Sample	Crystallite Diameter from XRD (nm)
NM-110	41.5
NM-111	33.8
NM-112	24.1
NM-113	41.5

In addition, CSIRO, 2012 investigated the crystallite size of the nanomaterials. Two methods were used to estimate average crystallite size based on XRD results.

Crystallite size of the test samples were calculated using Scherrer's formula ($D_{S\text{-}XRD}$) and through Rietveld refinement of the diffraction data ($D_{R\text{-}XRD}$). Comparison of crystallite/particle sizes in samples NM-110, NM-111, NM-112 and NM-113, as determined from XRD analyses are given in

Table 10.

Table 10: Crystallite size as determined from the XRD pattern

Sample	$D_{R\text{-}XRD}$ (nm)	$D_{S\text{-}XRD}$ (nm)
NM-110	113	41
NM-111	83	34
NM-112	43	25
NM-113	200	42

The crystallite size of the test samples determined in two independent experiments calculated using Scherrer's formula were comparable for all nanomaterial samples. The crystallite sizes determined by XRD were in the range of 24 nm (NM-112) to 42 nm. Both NM-110 and NM-113 have the same crystallite size of 42 nm. The average crystallite size determined by Rietveld refinement yielded larger crystallite sizes. This result could be explained by the fact that the Scherrer's formula ignores the contributions of width broadening due to strain and instrument effects. If these contributions are non-zero, the crystallite sizes could be larger than those predicted by the Scherrer formula, as revealed by Rietveld refinement of the diffraction data ($D\text{-}_{R\ XRD}$). These data were regarded as most reliable.

The Australian Deakin University, 2012 investigated the crystallite size of the nanomaterials but only results were provided. The crystallite size was reported to be 24 nm for NM-110, 21 nm for NM-111, 21 nm for NM-112 and 27 nm for NM-113 respectively.

It was shown that the crystallite size strongly depends on the used method. Using the same method comparable results were achieved. Taking all data into account it was shown that NM-112 has the smallest crystallite size diameter of all NMs. Based on the data using Scherrer's formula NM-110 and NM-113 have comparable crystallite size but this was not supported by Rietveld refinement of the diffraction data. Thus, there remains an uncertainty and further investigations were considered necessary to for a final conclusion on crystallite size.

Specific surface area

NPL, 2010 investigated the specific surface area of the NMs using BET Multipoint Specific Surface Area (SSA) determination. BET surface area measurements were determined using Autosorb-1 (Quantachrome Instruments). The Autosorb-1 was calibrated using a quartz rod of a known volume, which is traceable to NIST. This calibration was then further checked using two BAM certified reference materials: BAM-PM-

102 (nominal SSA 5.41 m^2/g) and BAM-PM-104 (nominal SSA 79.8 m^2/g). These two reference materials allowed the range of SSA of the nanoparticles to be encompassed with known specific surface area materials, thus adding confidence to the measurements. Surface area measurements were acquired using an 11-point BET gas adsorption method, with nitrogen as the adsorbate. Prior to analysis, the powdered sample was transferred to a sample bulb, then sealed and subsequently de-gassed overnight at 300 °C under a high vacuum and subsequently weighed on an analytical balance in order to determine the sample mass after the degassing step. The specific surface area was determined as follows:

Table 11: Specific surface area

Sample	Mean BET SSA (m^2/g)
NM-110	12.4 ± 0.6
NM-111	15.1 ± 0.6
NM-112	27.92 ± 1.2
NM-113	6.2 ± 0.3

CSIRO, 2012 investigated the specific surface area of the nanomaterials. BET Surface Area was determined using a Micromeritics Tristar II 3020 which uses physical adsorption and capillary condensation principles to obtain information about the surface area and porosity of a solid material. Prior to analysis, the powdered sample was transferred to a sample bulb, which was then sealed and de-gassed overnight at 300 °C under a high vacuum, and subsequently weighed on an analytical balance in order to determine the sample mass after the degassing step. Then the sample tube containing degassed sample was cooled to 77 K (the temperature of liquid nitrogen) and exposed to the analysis gas (nitrogen) at controlled pressures. With each incremental pressure increase, the number of gas molecules adsorbed on the surface increases. The equilibrated pressure (P) was compared to the saturation pressure (P_0) and their relative pressure ratio (P/P_0) was recorded along with the quantity of gas adsorbed by the sample at each equilibrated pressure. Experiments were done in duplicate, on different days. The values (±SD) were averaged from data obtained from duplicate experiments performed on different days. The specific surface areas of the ZnO samples, NM-110, NM-111, NM-112 and NM-113, obtained by the BET gas adsorption technique are provided in Table 12. The data represent the means of values (±SD) acquired on different days.

Table 12: Specific surface area

Sample	Mean BET SSA (m^2/g)
NM-110	11.76 ± 0.55
NM-111	13.75 ± 0.23
NM-112	27.25 ± 0.5
NM-113	5.78 ± 0.05

The MCA Cambridge, 2011 investigated the specific surface area of the nanomaterials. A Micromeritics TriStar II (3020) was used for the collection of nitrogen adsorption / desorption isotherm data up to a saturation pressure of approximately 0.995 P/P_0. The analysis was typically conducted to measure 45 adsorption relative pressure points and 23 desorption relative pressure points. Samples were outgassed overnight in vacuum at 300 °C using a Micromeritics VacPrep apparatus prior to analysis. In order to indicate any possible microporous nature of the materials additional relative pressure data were also collected at pressures lower than the usual starting point for analyses using this instrument. These were in the approximate range 0.005 to 0.01 P/P_0. Whilst the data reduction methods available are unsuitable for application to the micropore range the characteristic shape of the adsorption isotherm at these low partial pressures would provide a good indication of the presence of micropores in the sample material. The sample tube dead space was measured for each analysis using helium (CP grade) thus providing warm and cold freespace values. BET surface area was calculated using partial pressures in the nominal range 0.07 to 0.25. The results are presented in Table **13**.

Table 13: Results of the BET measurements

Sample	Multipoint surface area by Nitrogen (m^2/g)	BET C-value
NM-110	11.91± 0.0041	234
NM-111	14.62± 0.0483	21
NM-112	27.15 ± 0.0199	252
NM-113	4.33 ± 0.0011	198

NPL, 2010 investigated the specific surface area of the nanomaterials using BET Multipoint Specific Surface Area (SSA) determination. A Micromeritics TriStar II (3020) was used for the collection of nitrogen adsorption/desorption isotherm data up to a saturation pressure of approximately 0.995 P/Po. The analysis was typically conducted to measure 45 adsorption relative pressure points and 23 desorption relative pressure points. Samples were outgassed overnight in vacuum at 300 ° C using a Micromeritics VacPrep apparatus prior to analysis. In order to indicate any possible microporous nature of the materials additional relative pressure data were also collected at pressures lower than the usual starting point for analyses using this instrument. These were in the approximate range 0.005 to 0.01 P/Po. The sample tube dead space was measured for each analysis using helium (CP grade) thus providing warm and cold freespace values. Samples requiring only BET surface area analysis were analysed using the same equipment with the application of the same freespace measurement technique. BET surface area was calculated using partial pressures in the nominal range 0.07 to 0.25.
The results for both samples imply the samples are homogenous, all the results for the repetitions of each stub have high repeatability and are very close to the mean SSA results for NM111 and NM110: 15.41 ± 0.2005 and 11.96 ± 0.0665 m^2/g respectively.

All four methods using comparable analytical parameter were considered as suitable to address the endpoint. Taking all data into account, it was shown that NM-112 has the highest specific surface area of

all NMs (twofold higher than NM-110 and NM-112 and six-fold higher than NM-113). The specific surface area of NM-110 and NM-111 are in the same range and threefold higher than NM-113. In addition these data are in good correlation with the determined particle size (see chapter 0) and shape (see chapter 0) of the nanomaterials.

Zeta potential

CSIRO, 2012 investigated the Surface charge (zeta potential) of the nanomaterials. Zeta potentials of the samples were determined at different pH values (pH=2, 4, 6, 8 and 10) using a Brookhaven particle size analyser 90Plus equipped with a 657 nm laser. 10 mg. ZnO nano samples were dispersed in a cuvette containing 3 mL deionized water, and the pH was adjusted by adding either 0.1 M HCl or 0.1 M NaOH. The cuvette was placed in an ultrasonic bath for 10 seconds and then shaken manually to ensure good dispersion of particles in the sample. The electrode was inserted into the dispersion and the Zeta potential at each pH was measured 5 times and an average was determined. The temperature of all measurements was maintained at 25 °C. The results are presented in Table 14.

Table 14: Zeta potentials for ZnO samples dispersed in deionized water

pH	NM-110 Zeta potential (mV)	NM-111 Zeta potential (mV)	NM-112 Zeta potential (mV)	NM-113 Zeta potential (mV)
2.10	25.04 ± 1.84	14.36 ± 3.01	24.04 ± 1.91	16.94 ± 2.74
4.00	-1.50 ± 0.6	-33.67 ± 2.76	10.20 ± 0.92	5.94 ± 3.1
6.20	-5.79 ± 0.61	-26.78 ± 1.77	3.74 ± 0.56	-5.51 ± 0.72
8.10	-21.63 ± 0.82	-28.20 ± 1.5	-22.00 ± 3.45	-13.50 ± 0.76
10.00	-31.45 ± 0.48	-19.25 ± 1.06	-33.34 ± 0.62	-37.38 ± 1.25

The result showed the relationship between zeta potential and pH for the four ZnO samples tested. The isoelectrical point (IEP) was 3.9 for NM-110, 6.5 for NM-112 and 5.1 for NM-113. IEPs in the range 4-6 are consistent with the dissociation of water to H+ and OH- on the particle's surface and, where there is no surface coating, the IEP will be due solely to this dissociation. This therefore it was concluded that there is no specific surface coating on NM-110, NM-112 and NM-113. The IEP of NM-111 was determined to be 2.7 which was significantly lower than IEPs determined for the uncoated test samples. NM-111 is hydrophobic and observed to be very difficult to disperse in aqueous solutions; it is difficult to reconcile this observation with measurements of large zeta potential in water at most pHs. One possible explanation may be that the zeta potential data pertain to a small portion of the sample that is able to disperse. Therefore these data on zeta potential for NM-111 should not be considered as representative.

Furthermore, NPL, 2010 investigated the surface charge (zeta potential) of the NMs. Electrophoretic measurements were obtained using a Zetasizer Nano ZS (Malvern Instruments, UK) equipped with a 633 nm laser. The reference standard (DTS1230, zeta-potential standard from Malvern) was used to qualify the performance of the instrument. The results are given in Table 15.

Table 15: Zeta potentials for ZnO samples dispersed in different media

Sample	Deionized water (mV)	Deionized water + 5 mM NaCl (mV)	Fish medium (mV)	Seawater (mV)	Daphnia medium (mV)
NM-110	24.3 ± 0.4	20.8 ± 0.8	10.8 ± 0.1	N/A	1.3 ± 0.2
NM-112	24.6 ± 0.4	25.2 ± 0.6	12.4 ± 0.3	N/A	4.9 ± 0.2
NM-113	20.2 ± 0.4	13.9 ± 0.6	4.4 ± 0.4	N/A	-4.6 ± 0.4

Results show that zeta-potential values of NMs when dispersed in seawater cannot be successfully measured (due to high conductivity).

Results indicated high zeta-potential values for NMs that were dispersed either in deionized water (or deionized water + 5 mM NaCl), and thus confer stability in such media. Results showed values of zeta-potential measured were lower when the NMs were dispersed in an ecotoxicology media indicating much poorer dispersion stability in such media.

It was shown results of the two individual experiments were not consistent. The determined zeta-potentials in the NPL study in deionized-water are comparable to the zeta-potentials pH=2 solutions used in the CSIRO study. Due to the missing detailed description of the sample preparation the assessment of the different result could be achieved. As shown before, the NM highly agglomerates in deionized-water and sample preparation has a significant influence on the zeta-potential. Furthermore the surface charge of a given particle may be dependent both on pH and solution composition. The test conditions of both studies are significantly different and thus the data cannot be compared. Thus, without further experimental investigation the current results were regarded as not valid or sufficient for a reliable assessment.

Surface chemistry

CSIRO, 2012 investigated the surface chemistry, in particular the elemental composition near the surface of nanomaterials. Therefore an X-ray photoelectron spectroscopy (XPS) measurement of the test items was conducted. Spectra were obtained by irradiating the sample with an X-ray beam while simultaneously measuring the kinetic energy and number of electrons that escape from the top 1-10 nm layer of the material being analysed.

Table 16: Surface elemental composition measured in 8 weeks apart

Element	NM-110 (At. %)	NM-111 (At. %)	NM-112 (At. %)	NM-113 (At. %)
Zn	42.86 (39.57)	38.55 (35.49)	45.33 (41.48)	43.46 (38.88)
O	35.92 (40.54)	34.19 (36.92)	34.93 (41.83)	35.72 (38.41)

Element	NM-110 (At. %)	NM-111 (At. %)	NM-112 (At. %)	NM-113 (At. %)
C	20.29 (19.43)	27.25 (27.59)	18.21 (16.21)	20.00 (22.23)
Cl	0.92 (0.46)	n.d.	1.53 (0.48)	0.82 (0.48)

In all samples, zinc, oxygen and carbon were the major species present, with minor traces of chlorine detected in NM-110, NM-112 and NM-113 but not NM-111. The ratios of Zn:O was near, but not quite, stoichiometric typically with a deficiency of oxygen. The significant level of carbon present is likely due to surface contamination (the technique is sensitive to contaminations) or carbon-containing species adsorbed on the surface. However, NM-111 had significantly more carbon than the other samples, consistent with the fact that it has a triethoxycaprylylsilane surface coating. There appeared to be little change over the 8 week period except that data from the second experiment were noticeably closer to ZnO stoichiometry than the first determination.

In addition, NPL, 2010 determined the elemental composition of the different nanomaterials as measured by XPS. XPS measurements were obtained in ultra-high vacuum using a Kratos AXIS Ultra DLD (Kratos Analytical, UK) instrument fitted with a monochromated Al K-source, which was operated at 15 kV and 5 mA emission. Photoelectrons from the top few nanometers of the surface were detected in the normal emission direction over an analysis area of approximately 700 x 300 micrometres. Spectra in the range 1400 to –10 eV binding energy and a step size of 1 eV, using pass energy of 160 eV were acquired from selected areas of each sample. The peak areas were measured after removal of a Tougaard background. The manufacturer's intensity calibration and commonly employed sensitivity factors were used to determine the concentration of the elements present. High resolution narrow scans of some of the peaks of interest were acquired with a step size of 0.1 eV and 20 eV pass energy. (The manufacturer calibrated the intensity calibration over the energy range). The energy scale was calibrated according to ISO 15472. The charge neutraliser was used when acquiring the spectra, which shifted the peaks, by several eV. The carbon 1s hydrocarbon peak (285 eV binding energy) was used to determine the shift for identifying the peaks. Samples were prepared using carbon adhesive tape to affix them to 1 cm copper squares. Care was taken to cover the tape with the powders as completely as possible but some samples had better coverage than others and in a lot of cases there were a signal detected from the tape as well as the powder itself. The tape contained oxygen and silicon in addition to carbon.

Table 17: Results from the XPS measurements

Sample	C 1s (%)	O 1s (%)	Si 2s (%)	Zn $2p_{3/2}$ (%)
NM-112	64.7	26.9	0.0	8.4
NM-111	67.9	24.3	3.5	4.3
NM-113	25.6	44.3	0.0	30.1

Sample	C 1s (%)	O 1s (%)	Si 2s (%)	Zn $2p_{3/2}$ (%)
NM-110	69.0	25.1	0.3	5.

As evident from the results, there was a significant contribution of carbon and this can be largely attributed to contamination on the particles. Areas of best coverage were selected for analysis and, using XPS analysis of the carbon tape alone which showed a composition of 74% C, 21% O and 5% Si. Due to the lack of any significant signal from Si on samples, it was estimated that there was a better than 90 % coverage within these analysis areas. XPS also showed the presence of Si mainly associated with NM-111 sample i.e. Si 2s of 3.5 %. This can be attributed to the fact that this sample was coated with triethoxycapryl silane. The silicon contribution with NM-110 of 0.3 % is lower than the estimated detection limit for Si of ~ 0.5% and can be regarded as within the analytical noise level.

In addition, NPL, 2010 determined the elemental composition of the different nanomaterials as measured by XPS. XPS measurements were obtained in ultra high vacuum using a Kratos AXIS Ultra DLD (Kratos Analytical, UK) instrument fitted with a monochromated Al Kasource, which was operated at 15kV and 5mA emission. Photoelectrons from the top few nanometres of the surface were detected in the normal emission direction over an analysis area of approximately 700 x 300 micrometres. Spectra in the range 1400 to –10 eV binding energy and a step size of 1 eV, using pass energy of 160 eV were acquired from selected areas of each sample. The peak areas were measured after removal of a Tougaard background. The manufacturer's intensity calibration and commonly employed sensitivity factors were used to determine the concentration of the elements present. High resolution narrow scans of some of the peaks of interest were acquired with a step size of 0.1 eV and 20 eV pass energy. (The manufacturer calibrated the intensity calibration over the energy range). The energy scale was calibrated according to ISO 15472 Surface chemical analysis – X-ray photoelectron spectrometers – Calibration of energy scales. However, the charge neutraliser was used when acquiring the spectra, which shifted the peaks, by several eV. The C 1s hydrocarbon peak (285 eV binding energy) was used to determine the shift for identifying the peaks. Samples were prepared using carbon adhesive tape to affix them to 1 cm copper squares. Care was taken to cover the tape with the powders as completely as possible but some samples had better coverage than others and in a lot of cases there were a signal detected from the tape as well as the powder itself. The tape contained oxygen and silicon in addition to carbon.

The elemental compositions of the sub-sampled BASF powders for: a) Z-COTE and b) Z-COTE HP 1. The powders were adhered on to an (adhesive) carbon tape, in which the elemental composition of the tape was shown to be (atomic %) 74.3% C, 20.9% O, 4.8% Si. It is clear from the table of results that there is significant carbon and oxygen signal for both Z-COTE and Z-COTE HP1, which potentially originates from the carbon tape on which the NMs were fixed. Although the area (analysis area of ~ 700 x 300 µm, with information depth of ~ 8nm) was carefully chosen to obtain maximum particle coverage, it is clear that the carbon and oxygen tape background signal is contributing towards the XPS signal. Nonetheless, it was deduced a clear significant difference in the XPS results between the two sets of vials The count rate of Zn peaks were always lower from NM-111 samples vs. NM-110 samples i.e. 4 to 11.5 kcps and 19 to 23 kcps, respectively. This was attributed to the presence of a triethoxycarpryl silane coating associated with

NM-111 samples. Furthermore the Si level was much higher (3.1 to 4.1 %) in NM-111 1 if compared to NM-110 (0 to ~1%). This was consistent with the presence of a silane coating with the former sample. The silicon signal contribution (of less than 1%) can be attributed to silicon background signal from the fixing tape.

Furthermore NPL, 2010 used Time of Flight Secondary Ion Mass Spectrometry (ToF-SIMS). ToF-SIMS analysis was performed with a Bi+ cluster primary beam (incident at 45° from the sample normal with an energy of 25 keV) to obtain high mass resolution mass spectra with an imaging resolution of approximately 5 μm. The ion beam is rastered over an area of 500 μm × 500 μm using a 256 × 256 pixel raster. The ion beam current was measured before and after each sample was analysed. The raw data recorded consisted of a ToF-SIMS mass spectrum at every pixel. Data analysis was carried out retrospectively from the raw data using ION-TOF Surface Lab 6.1 software. The result was regarded as unreliable and therefore was not taken into account.

NPL, 2010 determined the elemental composition of the different nanomaterials as measured by XPS. XPS measurements were obtained in ultra high vacuum using a Kratos AXIS Ultra DLD (Kratos Analytical, UK) instrument fitted with a monochromated Al K alpha source, which was operated at 15kV and 5mA emission. Photoelectrons from the top few nanometres of the surface were detected in the normal emission direction over an analysis area of approximately 700 x 300 micrometres. Spectra in the range 1400 to –10 eV binding energy and a step size of 1 eV, using pass energy of 160 eV were acquired from selected areas of each sample. The peak areas were measured after removal of a Tougaard background. The manufacturer's intensity calibration and commonly employed sensitivity factors were used to determine the concentration of the elements present. High resolution narrow scans of some of the peaks of interest were acquired with a step size of 0.1 eV and 20 eV pass energy. (The manufacturer calibrated the intensity calibration over the energy range). The energy scale was calibrated according to ISO 15472 Surface chemical analysis – X-ray photoelectron spectrometers – Calibration of energy scales. However, the charge neutraliser was used when acquiring the spectra, which shifted the peaks by several eV. The C 1s hydrocarbon peak (285 eV binding energy) was used to determine the shift for identifying the peaks. The pellets of the sample powders were produced using the KBr Quick Press pellet presser. The powder was loaded from half to ¾ filled and gently pressed before the 3 pieces were inserted into the socket of the pellet maker. The handle was carefully pressed until some resistance was felt, and when pressed downwards there was ~ 1. 5 cm gap between the stop-screw on the handle to the central body. After a few minutes the handle was released, and pressure re-applied twice more until the presser clicked three times in total. The 3 piece assembly was taken out and the pellet removed.

The experimentally determined elemental compositions for all materials For the NM-111 - ZnO HP1 sample Zinc, Oxygen and Silicon (the latter from the silane layer) were all detected. All samples showed a large amount of carbon probably adsorbed from the atmosphere. The percentage concentration of carbon is consistent in the region 30-32% except from 0803 sample, which is in the region 22-26%. The percentage levels of the other sub-samples are remarkable consistent varying only between 37 – 40 % for Oxygen, 39-31% for Zinc and 1.2 – 2.2 % for silicon. More Oxygen that Zinc was detected due to the oxygen in the silane layer.

For the NM-110 - ZnO sample Zinc and Oxygen were detected but no Silicon. In addition, Carbon was detected. More Oxygen was detected than expected considering the amount of Zinc (assume a 1:1 ratio from Zinc Oxide). The amount of Oxygen varied between 39-41% and Zinc from 35-39%.Carbon shows the greatest variability from 20 – 26%.

Overall, the provided data on surface chemistry are a starting point but further investigations are necessary. According to the OECD guidance a tiered approached is proposed. Thorough characterisation of the surface chemistry of a nanomaterial requires e.g. analysis of spectroscopy, interfacial analysis, toxicology (reactive oxygen species generation), surface complexation modelling and colloid chemistry. There were no studies provided with regard to these endpoints. Thus, a final conclusion on surface chemistry was not possible.

Dustiness

NPL, 2010 investigated the dustiness of the nanomaterials. The dustiness of the sample powder was carried out using the rotating drum method specified in the new European standard of the dustiness of bulk samples (EN15051). Three replicate tests of the powder were carried out to obtain an estimate of the precision of the measurements. The standard also requires simple moisture content measurements to be made for each material, as dustiness has been found to be a function of moisture content. Analysis was carried out at 50 + 5 % relative humidity. For each measurement 35 mL was tested.

Table 18: Mean and SD of the dustiness results and moisture content

Sample	Inhalable fraction (mg/kg)		Thoracic fraction (mg/kg)		Respirable fraction (mg/kg)		Moisture content (%)	
	Mean	SD	Mean	SD	Mean	SD	Mean	SD
NM-110	2905	371	599	239	27	3	0.5	0.10
NM-111	5880	610	1340	241	138	105	0.3	0.00
NM-112	1095	222	317	37	42	8	1.2	0.20
NM-113	166	26	34	10	10	2	0.4	0.10

Table 19: The dustiness classifications of the sample powders

Sample	Dustiness Classification		
	Inhalable	Thoracic	Respirable
NM-110	Moderate	Moderate	Low
NM-111	High	High	Moderate
NM-112	Moderate	Moderate	Low
NM-113	Very Low	Very Low	Low

Test results of the dustiness studies showed a significant difference in the inhalable dustiness levels (Table 19). The respirable dustiness index, however, was quite comparable and possibly influenced by larger variation than the inhalable dust fraction. The inhalable dustiness index is classified to be at the high end of "low" dustiness (NM-110) to just "moderate" (NM-111). This compares approximately to the levels of nanoparticle powders of goethite, organoclay and talc compared to dustiness data on other test nanomaterials. For respirable dust both samples are in the lower "moderate" dustiness range (range: 50 to 250 mg/kg).

Porosity

The porosity of the samples was investigated in three independent laboratories CSIRO, 2012, Deakin University, 2012 and NPL, 2012.

In the first study CSIRO, 2012, determined the porosity simultaneously with surface area using a Micromeritics Tristar II 3020 instrument. The Barrett-Joyner-Halenda (BJH) method for analysing gas adsorption and desorption isotherms was used to determine pore area, specific pore volume and pore size distribution independent of the external area due to the particle size of the sample.

Table 20: Results of the porosity determination

sample	t-Plot Micropore Surface Area: (m^2/g)	t-Plot External Surface Area : (m^2/g)	t-Plot micropore volume (cm^3/g)	BJH Desorption average pore width (4V/A): (nm)
NM-110	1.79315 ± 0.58	9.97 ± 0.98	0.000805 ± 0.00029	8.97445 ± 0.45
NM-111	0	20.899 ±0.312	0	20.802 ± 0.467
NM-112	5.3518 ± 0.85	21.9027 ± 1.17	0.0024255 ± 0.0004	15.763 ± 1.0
NM-113	1.38765 ± 0.66	4.39675 ± 0.11	0.000638 ± 0.11	10.749 ± 1.27

All samples have either low or no microporosity. The major contribution to total surface area is from external surfaces and is thus predominantly determined by particle size and shape rather than high internal porosity. For pristine samples of ZnO (NM-110, NM-112 and NM-113) the surface areas are generally consistent with those determined by the BET method. However, for NM-111 (the coated sample), the t-plot calculation indicates no micropore (pores smaller than 2 nm in diameter) surface area and an external surface area considerably greater than that determined by the BET method (~21 m^2/g cf 14 m^2/g). This variation is likely due to the presence of the hydrophobic (mesoporous) silicone coating which has capacity to adsorb gas both internally and externally and imply a greater surface area. The fact that no microporous volume is reported suggests that any porosity is likely mesoporous (pores greater than 2 nm and less than 50 nm in diameter). Consequently, for the coated sample only, the t-plot external surface area (multi-layer) calculation is higher than the BET specific surface area (monolayer) calculation.

In the second study Deakin University 2012 investigated the porosity of the samples were using a Micromeritics Tristar 3000 apparatus. The Barrett-Joyner-Halenda (BJH) method for analysing gas adsorption and desorption isotherms was used to determine pore area, specific pore volume and pore size distribution independent of the external area due to the particle size of the sample.

Table 21: Results of the porosity determination

Sample	Specific Surface Area (m^2/g)	Pore Volume (cm^3/g)	Average pore width (nm)
NM-110	6.6 ± 0.3	0.0100	6.1
NM-111	11.8 ± 0.2	0.0289	8.2
NM-112	25.9 ± 0.3	0.0652	10
NM-113	4.0 ± 0.15	0.00655	6.5

The scale of average pore width indicates that the quantity of meso-pores in in primary particles are negligible and that the measured pore size distribution reflects the pores in the agglomerates (secondary particles). All samples have very low microporosity. The major contribution to total surface area is from external surfaces and is thus predominantly determined by particle size and shape rather than high internal porosity. NM-112 has the highest surface area and micropore volume of all the samples approximately 3-4 times greater than other samples.

In the third study the MCA in Cambridge, 2011 determined the porosity of the NMs. A Micromeritics TriStar II (3020) was used for the collection of nitrogen adsorption / desorption isotherm data up to a saturation pressure of approximately 0.995 P/P_0. The analysis was typically conducted to measure 45 adsorption relative pressure points and 23 desorption relative pressure points. Samples were outgassed overnight in vacuum at 300 °C using a Micromeritics VacPrep apparatus prior to analysis. In order to indicate any possible microporous nature of the materials additional relative pressure data were also collected at pressures lower than the usual starting point for analyses using this instrument. These were in the approximate range 0.005 to 0.01 P/P_0. Whilst the data reduction methods available are unsuitable for application to the micropore range the characteristic shape of the adsorption isotherm at these low partial pressures would provide a good indication of the presence of micropores in the sample material. The sample tube dead space was measured for each analysis using helium (CP grade) thus providing warm and cold freespace values. Samples requiring only BET surface area analysis were analysed using the same equipment with the application of the same freespace measurement technique. BET surface area was calculated using partial pressures in the nominal range 0.07 to 0.25.

The pore size distribution is presented as pore size by volume and area from the adsorption isotherm using the BJH method. The pore size distribution data presented in the BJH reports is applied to a maximum of 1000 Å. The total pore volume of the materials is calculated from the volume of nitrogen adsorbed at the maximum relative pressure obtained on the adsorption branch of the isotherm. The results are presented in Table 22**: porosity measurements** :

Table 22: porosity measurements

Sample	Porosity (cm^3/g)
NM-110	0.041538
NM-111	0.071347
NM-112	0.158354
NM-113	0.013820

Overall, the provided data has some limitation regarding validity and reliability and serves for orientation only. In general, the porosity is a dimensionless value and should be expressed as value between 0 and 1 or as percentage between 0 and 100%. None of the available study reports has reported the porosity in this recommended manner. However, all samples have either low or no microporosity. The major contribution to total surface area is from external surfaces and is thus predominantly determined by particle size and shape rather than high internal porosity. For samples NM-110, NM-112 and NM-113 the surface areas are generally consistent with those determined by the BET method. Data for NM-111 were inconsistent (cf Table 20 and Table 21).

Pour (Bulk) density / Tapped Density / Carr Index

Escubed Ltd., 2012 determined the density of the nanomaterials using a Copley JV2000. A known mass of the dry sample was placed into a measuring cylinder to a recorded volume and tapped by mechanically raising and lowering by a set distance until a consistent volume was reached, which corresponds to the maximum packing density of the material. The Carr Index was calculated from the respective bulk and tapped densities.

Table 23: Results of the density measurements

Sample	Bulk Density (g/cm3)	Tapped Density (g/cm^3)	Carr Index
NM-110	0.293	0.346	15.351
NM-111	0.693	0.832	16.799
NM-112	0.415	0.519	20.000
NM-113	0.646	0.714	9.471

NM-110 and NM-111 have comparable particle size. NM-112 was determined to have the smallest particle size compared to the other 3 nanomaterials and NM-113 (“bulk material”) was determined to have the largest particle size. As the particle size directly influence the tapped density, this general trend should be observed in the density measurements. The provided results for density are not consistent with the data on particle size which were in general regarded as reliable. This, inconsistence might be caused by different parameter (e.g. sample preparation, representative sample). Thus, it was not possible to finally conclude on pour density.

Photocatalytic activity

The Deakin University, 2012 investigated the photocatalytic activity by monitoring the degradation of Rhodamine B (RhB) in aqueous solutions having the concentration of 0.0096g/L. To quantify the photo-reactivity, the absorbance at 554 nm (the wavelength of maximum absorbance for RhB) was monitored. The results were as follows:

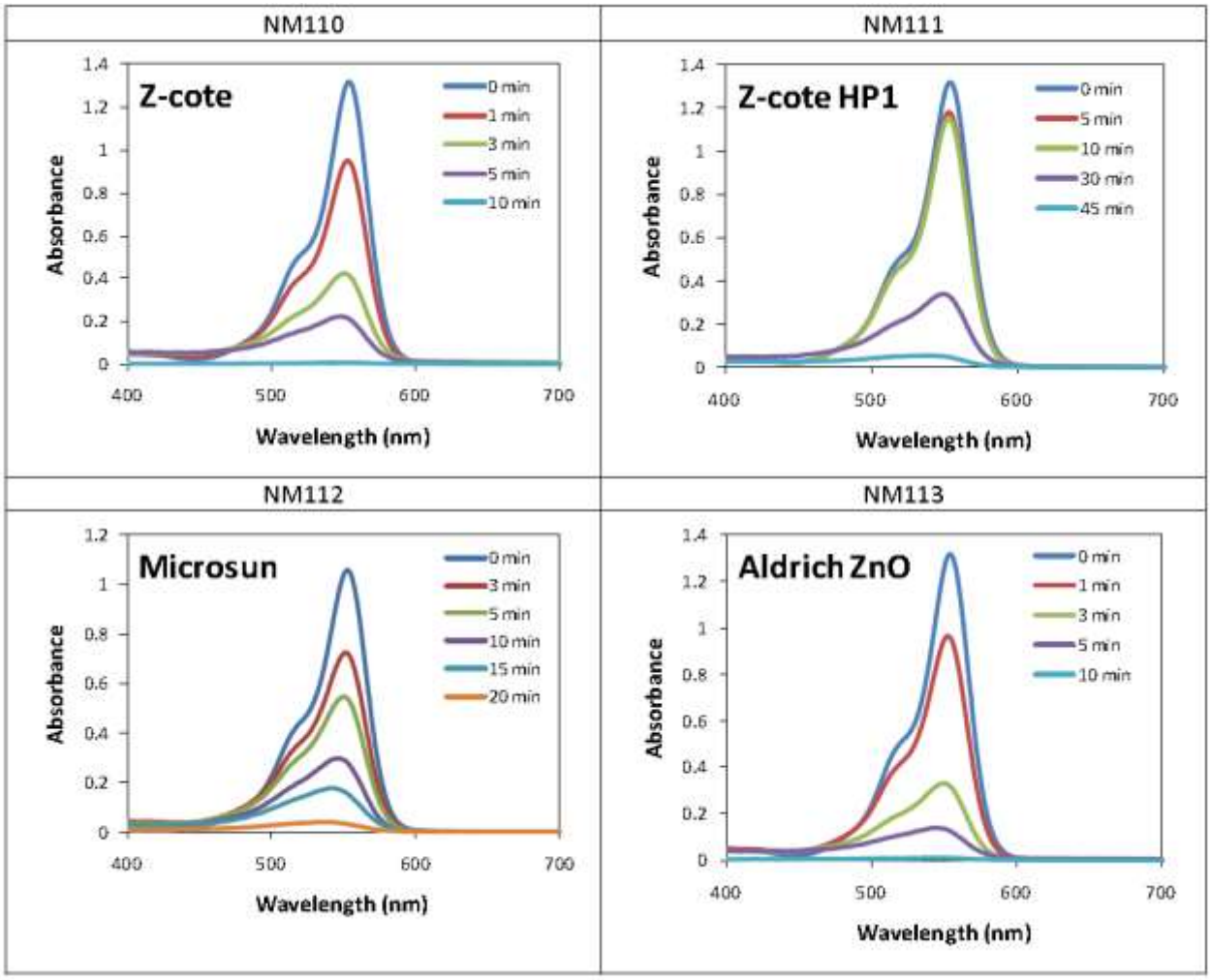

Figure 9: Optical absorption peak of Rhodamine-B

Table 24: Results of photocatalytic activity expressed as rate constant

Sample	Rate constant (1/min)
NM-110	0.4765
NM-111	N/A*
NM-112	0.1502
NM-113	0.44635

*Not available due to surface coating

NM-111 did not show the first order kinetics due to the presence of a surface coating. The rate constant did not show a strong correlation with specific surface are. The photocatalytic activity of NM-0113 was as high as NM-110. When the photoactivity rates are normalised with specific surface area values, NM-110 showed the highest photocatalytic activity per unit surface area. NM-112 is the sample with the smallest primary particle size (and highest surface area), and its photocatalytic activity is less than that of its larger counterpart NM-110, and NM-113 with the largest particle size. The results could be explained as surface defects acting as charge recombination sites to prevent photocatalysis. NM-112 has near spherical shapes that are expected to have a large number of surface defects. On the other hand, MN110 and MN113 have geometrical shape particles that indicate high crystallinity and a low number of surface defects results in higher photocatalytic activities.

Furthermore CSIRO, 2012 investigated the photocatalytic activity by monitoring the degradation of 1,1-diphenyl-2-picrylhydrazyl (DPPH) in mixtures of 1:1 Mineral Oil White Light : Caprylic Capric C8/C10 Triglyceride (MOTG), following the procedure described by Dransfield et al., 2000. To quantify the photo-reactivity, the absorbance at 520 nm (the wavelength of maximum absorbance for the purple DPPH radical) was monitored. The data were analysed by comparing (i) the decay time (the time required to bleach the dye) and (ii) the first order rate constant of the radical consumption calculated by using the linear relationship between $\ln(c/c_0)$ and irradiation time t. A shorter decay time and larger rate constant corresponds to higher photocatalytic activity.

In addition to charge transfer and subsequent radical formation, recombination of separated electrons and surface defects in/on the ZnO particle may be effective in suppressing photocatalytic activity. Theoretically, photocatalytic activity should decrease with increasing particle size (or decreasing surface area) because recombination processes dominate at larger sizes. However, the expected correlation between surface area and photocatalytic activity was not supported by the data.

Table 25: Results of the measurements of the photocatalytic activity

Sample	Decay time (min)	Rate constant (1/min)
NM-110	9	0.124
NM-111	11	0.112
NM-112	11	0.069
NM-113	15	0.089

NM-112 is the sample with the smallest primary particle size (and highest surface area), and yet its photocatalytic activity is less than that of its larger counterpart NM-110, and comparable to NM-113 with the largest particle size. The influence on photocatalytic activity of the combination of radical surface recombination and surface migration rates with availability of surface adsorbed species may be greater than that of volume recombination. A comparison of the data for the samples NM-110 (uncoated) and NM-111 (similar size to NM-110 but with a surface coating), indicates that the presence of a surface coating appears to mitigate, but not eliminate, photocatalytic activity.

The results (e.g. rate constants) were not directly comparable as the photocatalytic activity of the ZnO samples was determined by monitoring the degradation of two different dyes in different media (aqueous, organic). Nevertheless it was shown that under the different test conditions the photocatalytic activity of the coated nano-material (NM-111) was significantly different (means lower) compared to the other three ZnO samples. Furthermore it was shown that photocatalytic activity of the NM-113 ("bulk material") is comparable with the other uncoated nano ZnO samples indicating no differences in photocatalytic activity between bulk and nano ZnO. Based on the provided data no further conclusion could be made.

Radical formation potential

NPL, 2010 investigated the radical formation potential. The test items were dispersed in four different media in the presence of KI (deionized water, seawater, daphnia and fish media) and the dispersions were exposed for 60 minutes, under 1000 W/m^2 white light irradiation. Anatase (TiO_2) was used as positive control. Results showed that there was a certain level of tri-iodide (I_3-) measured in the irradiated sample. Tri-iodide was suppressed in seawater and may be attributed to a higher concentration of ions in this media. Results for Anatase (TiO_2), being the most active photocatalytic material, show a much higher rate of tri-iodide formation than the corresponding zinc oxide NMs. In particular, the absorbance signal was highest in deionized water, lower in daphnia and fish media and when in seawater, the absorbance signal was reduced (as in the corresponding blank i.e. seawater with no Anatase). It was shown that the absorbance signal of NM-111 is much higher in seawater than when dispersed in the other three media. In the course of the present study no explanation was found. In general, for the ZnO nanomaterials the absorbance signals were within a similar range to that of the corresponding irradiated blank (Samples that were kept in the dark exhibited no absorption peak at 352 nm) indicating no differences Radical formation potential between bulk and nano ZnO.

Overall summary and conclusion nanomaterial specific physical and chemical properties of the ZnO NM

The primary intention of the nano specific investigations on the physical and chemical properties of the OECD nanomaterials, NM-110, NM-111, NM-112, and the bulk product NM-113 was to enable an assessment on the comparability of these materials.

However, it has to be taken into consideration that at the time point of performance of these investigations, there were no validated OECD guidelines (or comparable standard) available for most of the endpoints addressed in the above section.

The studies were conducted in the course of the UK's PROSPEcT/OECD programme. Some parameters (e.g. shape, specific surface area particle size) are better-defined and more straightforward to measure than others. For other complex parameters, a certain degree of method development and standardisation will be required. All provided studies were not conducted under GLP conditions. The studies were performed in the course of the years 2010 and 2012. In the meantime, further works in the OECD program were conducted and further publications in the Series on the Safety of Manufactured Nanomaterials are available. In addition the ECHA has published in the meantime (April 2012) several guidance documents with respect nanomaterials. The provided data were evaluated with respect to current guidelines and recommendations (as of June 2015, see 2. Introduction).

Thus, it has to be taken into consideration that data in the table below are provided for orientation to enable a preliminary comparative overview as several data (in italic) rely on limited documentation and deficiencies, when compared e.g. to ECHA and OECD guidance documents.

Table 26: Summary of nanomaterial specific physical and chemical properties of the ZnO NM

Property	Value	Sample	Reference
Shape	polyhedral particles with quite variable particles morphology	NM-110	CSIRO, 2012 NPL Report AS 53 Deakin University ,2012
	polyhedral with quite variable morphology	NM-111	
	spherical particles	NM-112	
	polyhedral particles with quite variable particles morphology	NM-113	
Dissolution	*dissolving the fastest*	NM-110	CSIRO, 2012 NPL Report AS 53
	-	NM-111	
	dissolving the slowest	NM-112	
	-	NM-113	
Particle size distribution	*77.5 ± 18 nm*	NM-110	CSIRO, 2012
	75.2 ± 7.6 nm	NM-111	
	33.75 ± 6.2 nm	NM-112	
	149.7 ± 25 nm	NM-113	
Thermal stability	*lowest weight losses*	NM-110	CSIRO,

Property	Value	Sample	Reference
	highest weight losses	NM-111	2012
	exhibited minor weight losses	NM-112	
	higher weight losses	NM-113	
Redox potential	No reliable data	NM-110	
	No reliable data	NM-111	
	No reliable data	NM-112	
	No reliable data	NM-113	
Agglomeration/ aggregation	*highly agglomerated and aggregated and consisted of polydisperse distributions of particles*	NM-110	CSIRO, 2012
		NM-111	
		NM-112	
		NM-113	
Crystalline phase	hexagonal wurtzite zincite crystalline phase	NM-110	CSIRO, 2012 Deakin University, 2012
		NM-111	
		NM-112	
		NM-113	
Crystallite size	No conclusive data	NM-110	
	No conclusive data	NM-111	
	No conclusive data	NM-112	
	No conclusive data	NM-113	
Specific surface area	*12.4 ± 0.6*	NM-110	NPL Report AS 53
	15.1 ± 0.6	NM-111	
	27.92 ± 1.2	NM-112	
	6.2 ± 0.3	NM-113	
Zeta potential	No conclusive data	NM-110	
	No conclusive data	NM-111	
	No conclusive data	NM-112	
	No conclusive data	NM-113	
Surface chemistry	No conclusive data	NM-110	
	No conclusive data	NM-111	
	No conclusive data	NM-112	
	No conclusive data	NM-113	

Dustiness	Inhalable	Thoracic	Respirable		NPL Report AS 53
	Moderate	Moderate	Low	110	
	High	High	Moderate	111	
	Moderate	Moderate	Low	112	
	Very Low	Very Low	Low	113	
Porosity	No conclusive data			NM-110	
	No conclusive data			NM-111	
	No conclusive data			NM-112	
	No conclusive data			NM-113	
Pour density	No conclusive data			NM-110	
	No conclusive data			NM-111	
	No conclusive data			NM-112	
	No conclusive data			NM-113	
Photocatalytic activity	No conclusive data			NM-110	
	No conclusive data			NM-111	
	No conclusive data			NM-112	
	No conclusive data			NM-113	
Radical formation potential	No reliable data			NM-110	
	No reliable data			NM-111	
	No reliable data			NM-112	
	No reliable data			NM-113	

Finally and considering the deficiencies and limitations, it can be preliminary concluded that based on the available data on the physical and chemical properties, the nanomaterials N-110 and 111 can be considered as highly comparable and comparable to NM-112.

The shapes of the particle as well as the morphology of the NM-110, NM-111 and NM-113 were comparable. The three NM were described as polyhedral with variable morphology and size. The NM-112 was determined to be distinctly different to all the other samples. NM-112 was described to appears as near spherical and with the smallest particle size compared to the other three materials.
The basic assumption (NM-113 as “bulk material” has the largest particle size) could be confirmed by particle size determination. Throughout all measurements NM-112 was determined to have the smallest particle size compared to the other nanomaterials. The results of the different measurements of NM-110 and NM-111 samples showed that these 2 nanomaterials have a comparable particle size. This general trend was also observed for the endpoints density and surface area, which are directly linked to the particle size.

It was shown that the dissolution rates were fastest when the NMs were dispersed in deionized water, with NM-110 dissolving the fastest and NM-112 dissolving the slowest. Out of all ecotox media, fish medium

showed highest dissolution rate followed by daphnia and then seawater. Dispersing nanomaterials in such ecotox media would mean less stable dispersion and this subsequently equates to the reduced surface area concentrations and thus a lower dissolution rate. There was no significant difference in dissolution rate between the uncoated ZnO nanomaterials and the bulk material.

There were no differences observed regarding the thermal properties for the four nanomaterials. This property is not linked to the material form (nano or bulk) but to coating.

Analysis indicated that the all investigated zinc oxide nanomaterials were highly agglomerated and aggregated. The agglomeration was largest in seawater and smallest in deionized water indicating that larger agglomerates exist in ecotoxicology media. In all cases it was shown that the nanomaterials consisted of polydisperse distributions of particles.

It was shown that all materials were in a hexagonal wurtzite zincite crystalline phase, independent whether from bulk or nano. NM-112 has the smallest crystallite size diameter of all NMs. Some data indicated that NM-110 and NM-113 have comparable crystallite size but this was not supported a different analytical method. Thus, there remains an uncertainty.

NM-112 has the highest specific surface area of all nanomaterials (twofold higher than NM-110 and NM-112 and six-fold higher than NM-113). The specific surface area of NM-110 and NM-111 are in the same range and threefold higher than NM-113. In addition these data are in good correlation with the determined particle size (see chapter 3.4) and shape (see chapter 3.3) of the nanomaterials.

A final conclusion on the comparability regarding zeta potential, surface chemistry and pour density was not possible.

The respirable dustiness index was quite comparable for all nanomaterials and was possibly influenced by larger variation than the inhalable dust fraction. The inhalable dustiness index is classified to be at the high end of “low” dustiness (NM-110) to just “moderate” (NM-111). This compares approximately to the levels of nanoparticle powders of goethite, organoclay and talc compared to dustiness data on other test nanomaterials. For Respirable dust both samples are in the lower “moderate” dustiness range (range: 50 to 250 mg/kg).

It was shown, that all samples have either low or no microporosity. The major contribution to total surface area is from external surfaces and is thus predominantly determined by particle size and shape rather than high internal porosity. For samples NM-110, NM-112 and NM-113 the surface areas are generally consistent with those determined by the BET method but data for NM-111 were inconsistent.

Under the different test conditions the photocatalytic activity of the coated nano-material (NM-111) was shown to be significantly different (means lower) compared to the other three ZnO samples. Furthermore it was shown that photocatalytic activity of the NM-113 (“bulk material”) is comparable with the other uncoated nano ZnO samples indicating no differences in photocatalytic activity between bulk and nano ZnO. In general, for the ZnO nanomaterials the absorbance signals were within a similar range to that of the corresponding irradiated blank indicating no differences radical formation potential between bulk and nano ZnO.

Ecotoxicological Information on Zinc Oxide (ZnO) Nanomaterials (NM)

Aquatic Toxicity

Short-term toxicity to fish

In a non-GLP/guideline conform 96 h-embryo-larval bioassay according to Schulte & Nagel (1994), zebra fish (*Danio rerio*) embryos were exposed to non-OECD uncoated nanoscale ZnO (purity > 99%, particle size range: 50-360 nm) and the bulk counterpart ZnO/bulk (purity > 99%) at nominal concentrations of 0.1, 0.5, 1, 10 and 50 mg/L. Based on the mortality rate, the 96-h LC_{50} value of uncoated nanoscale ZnO and ZnO/bulk were 1.793 mg/L and 1.550 mg/L, respectively. The 84-h EC_{50} values, determined on basis of hatching rate, were 2.065 mg/L for uncoated nanoscale ZnO and 2.066 mg/L for ZnO/bulk (Zhu et al., 2008).

In conclusion, uncoated nanoscale and its bulk counterpart indicated comparable acute toxicity to zebra fish.

Long-term toxicity to fish

In a GLP-conform study following OECD 210 (Fish, Early-life Stage Toxicity Test), *Danio rerio* embryos were exposed to NM-110 (purity > 99%) for 35 days at nominal concentrations of 7, 20, 60, 180 and 540 µg/L as well as to the reference materials, NM-113 and ionic zinc (no details on purity), at a nominal concentration of 180 µg/L. The following table indicates the NOEC and LOEC of NM-110 based on nominal values.

Table 27: NOEC and LOEC of NM-110

End point	DPH[a]	NOEC[b] (µg/L)	LOEC[c] (µg/L)
Larval total length	32	≥ 540	> 540
Larval dry weight	32	≥ 540	> 540
Larval survival	32	≥ 540	> 540
Delay in hatching	< 7	≥ 60[d]	180[d]

[a]DPH = days post hatch
[b]NOEC = No-observed-effect concentration
[c]LOEC = Lowest –observed-effect concentration
[d]based on cumulative number of larvae hatching on day 4 and day 5

A slight delay in the hatching of larvae exposed to > 180 µg/L NM-110 was observed possible due to the result of a data bias from one replicate tank. Similar concentrations of NM-113 and ionic zinc (180 µg/L) indicated an inhibitory effect on growth compared to NM-110. Poor survival during the embryonic stage and immediately post hatching suggested that the batch of eggs used in this study were of poor quality. The post-hatch survival of control individuals was lower than the OECD recommended value of 75%.

However, no clear dose related effects following exposure to NM-110 in the concentration range tested were observed (Sanders et al. 2012).

Short-term toxicity to aquatic invertebrates

In a modified GLP-conform OECD 202 study, *Daphnia magna* was administrated with NM-112 and the reference materials NM-113 as well as ionic zinc for total exposure duration of 48 hours. Additionally, the feeding was assessed after 24 hours. The feeding rate of organisms exposed to 1 mg/L NM-112 was reduced up to 30% compared to the non-nano reference material. This effect was not related to a physical impairment or obstruction of the organism's feeding apparatus. Based on the mortality, the 48-h LC_{50} value of NM-112 and NM-113 were 1.55 mg/L and 3.32 mg/L, respectively (University of Exeter, Fabrega and Galloway, 2010). The toxicity to Daphnia magna of nanoscale NM-112 and NM-113 (bulk) was equal.

In a further guideline conform study, *Daphnia magna* was exposed for 48 hours to nominal concentrations of 0.01 – 100 mg/l with NM-110 (purity > 99%), NM-111 (purity 96-99%), Z-COTE MAX (purity 96-99%) or non-nanoscale ZnO (< 1 µm, Sigma-Aldrich, corresponding to NM-113) according to OECD 202. The following 48 hour EC_{50} values (nominal) based on the mobility were determined: 7.5 mg/L (NM-110), 1.1 mg/L (NM-111), 1.0 mg/L (Z-COTE MAX) and 1.0 mg/L (non-nanoscale ZnO). Additionally, the EC_{50} value of NM-111 diluted in well-spring surface water and pond surface water was determined. The use of water resulted in a decrease of acute toxicity (Wiench et al., 2009). Nanoscale ZnO was equal or less toxic than ZnO bulk.

The toxicity of non-OECD NM (nano-sized ZnO (particle size: 50-70 nm), bulk ZnO and $ZnSO_4 \cdot 7 H_2O$) was investigated to two crustaceans, *Daphnia magna* as well as *Thamnocephalus platyrus* under non-GLP/guideline conform conditions. No details on purity of the test items are indicated. The crustacea ecotox assays were performed according to the Standard Operational Procedures of Daphtoxkit F™ magna or Thamnoxkit F™, respectively. Using *Daphnia magna*, the following 48 h LC_{50} values were calculated: 3.2 mg/L (nano ZnO), 8.8 mg/L (bulk ZnO), and 6.1 mg/L ($ZnSO_4 \cdot 7 H_2O$). *Thamnocephalus platyrus* was more sensitive to tested substances. The following 24 h LC_{50} values were estimated: 0.18 mg/L (nano ZnO), 0.24 mg/L (bulk ZnO), and 0.98 mg/L ($ZnSO_4 \cdot 7 H_2O$) (Heinlaan et al., 2008). The results showed that the toxicity of nanoscale ZnO and ZnO bulk was almost identical with slightly more toxic effects of the nanoscale ZnO compared to bulk and ions.

In conclusion, the acute toxicity of NM-110, NM-111, NM-112 and of the reference item NM-113 to aquatic invertebrates was investigated in two OECD conform studies. NM-112 (LC_{50} 1.55 mg/L, based on mortality) was equal toxic to *Daphnia magna* compared to NM-113 (LC_{50} 3.32 mg/L, based on mortality). While the 48-h EC_{50} values (based on mobility) were comparable for NM-111 (1.1 mg/L) and non-nanoscale NM (1.0 mg/L), NM-110 showed an EC_{50} value of 7.5 mg/L. These slight differences may result from the different particle size and the use of coated and uncoated particles. However, the in principle results were very comparable to coated ZnO, uncoated ZnO and ZnO bulk.

Long-term toxicity aquatic invertebrates

There are no data available on chronic toxicity to aquatic invertebrates.

Toxicity to aquatic algae and cyanobacteria

A non-GLP/guideline conform study with non-OECD nanomaterial was conducted to characterize ZnO nanoparticles (nano-ZnO_{powder} and nano-$ZnO_{dispersant}$) by using dynamic light scattering (DLS), transmission electron microscopy (TEM), and equilibrium dialysis. Both, ZnO nanoparticles and bulk ZnO showed rapid dissolution in freshwater medium (pH 7.6) in a similar manner. The chronic toxicity of ZnO nanoparticles was examined in *Pseudokirchneriella subcapitata* in comparison to the reference items, $ZnCl_2$ and ZnO bulk. The toxicity experiments revealed comparable toxicity for nanoparticulate ZnO, bulk ZnO, and $ZnCl_2$, with a 72-h LC50 value near 60 µg/L, attributable solely to dissolved zinc (Franklin, 2007).

Toxicity to microorganisms

The inhibitory effect of NM-110 (purity 99.1%) on activated sludge was investigated in a 180-min static test according to OECD 209 under GLP conditions. The activated sludge was taken from a municipal wastewater treatment plant. NM-110 was tested at concentrations of 62.5, 125, 250, 500 and 1000 mg/L. No details on test item preparation are specified. Based on nominal concentrations, the EC_{50} and EC_{20} value was greater than 1000 mg/L. The EC_{10} value was determined to be 750 mg/L (BASF SE, 2012b). Since the EC_{20} value is > 100 mg/L, the inhibition of the degradation activity of activated sludge is not anticipated when introduced to biological treatment plants in appropriate low concentrations.

Adams (2006) examined the antibacterial activity of the non-OECD NM (ZnO powder; mean particle size 480 nm). *Bacillus subtilis* or *Escherichia coli* were exposed to nominal concentrations of 0.04 – 21.3 mg/L for 6 hours in suspension and afterwards cultures were plated onto Luria-Bertani plates and left grow for 14-20 h. Test solutions were prepared in Milli-Q® water without sonification. *E. coli* was less sensitive to the addition of ZnO nanoparticles than *B. subtilis*.

The most reliable study (BASF, 2012b) indicated an EC_{50} and EC_{20} value > 1000 mg/L and an EC_{20} of 750 mg/L for the uncoated nanoscale ZnO (NM-110).

Summary and conclusion – Aquatic toxicity

Acute aquatic toxicity of non-OECD nanomaterials (uncoated nanoscale and ZnO/bulk) or OECD nanomaterials (particularly NM-110, NM-111, NM-112, NM-113) was investigated in zebrafish (*Danio rerio*), *Daphnia magna* and in microorganisms, respectively. Long-term toxicity was only examined for NM-110 in the zebrafish, *Danio rerio*. In conclusion, the aquatic toxicity of nanoscale ZnO is comparable to ZnO bulk. With respect to the physical and chemical properties, NM-110, NM-111, NM-112, and NM-113 showed different agglomeration behaviour towards each other and in different media (deionized water, fish media, seawater, daphnia media). However, this difference in agglomeration behaviour did not cause differences in the aquatic toxicity of nanoscale ZnO and ZnO bulk materials.

The following table summarized the most reliable aquatic toxicity studies of ZnO nanomaterials in comparison to ZnO bulk material.

Table 28: Summary of relevant and reliable endpoints to acute and chronic aquatic toxicity

Organism/ Test duration	Test material	Results	Remarks	Reference
Acute toxicity - Fish				
Zebrafish (*Danio rerio*) 96-h	Uncoated nanoscale	96-h LC_{50}: 1.793 mg/mL (based on mortality) 84-h EC_{50}: 2.065 mg/L (based on hatching rate)	bioassay according to Schulte & Nagel (1994)	Zhu et al. (2008)
	ZnO/bulk	96-h LC50: 1.550 mg/mL (based on mortality) 84-h EC50: 2.066 mg/L (based on hatching rate)		
Long-term toxicity - Fish				
Zebrafish (*Danio rerio*) 35-d (flow-through)	NM-110	NOEC ≥ 540 µg/L and LOEC > 540 µg/L (32 DPH, nominal, larval survival, dry weight, total length) *NOEC ≥ 60 µg/L and *LOEC > 180 µg/L (< 7 DPH, nominal, delay in hatching)	OECD 210	Sanders et al., University of Exeter (2012)
Acute toxicity – Aquatic invertebrates				
Daphnia magna	NM-112	LC_{50} = 1.55 mg/L	modified OECD 202	Fabrega and Galloway, University of Exeter
	NM-113	LC_{50} = 3.32 mg/L		

Organism/ Test duration	Test material	Results	Remarks	Reference
48-h				(2010)
Daphnia magna 48-h	NM-110	EC_{50} = 7.5 mg/L	OECD 202	Wiench et al. (2009)
	NM-111	EC_{50} = 1.1 mg/L		
	Non-nanoscale ZnO < 1µm	EC_{50} = 1.0 mg/L		
Daphnia magna and 48-h	Nano ZnO (50-70 nm) Bulk ZnO	LC_{50} = 3.2 mg/L LC_{50} = 8.8 mg/L	Daphtoxkit F™ magna	Heinlaan et al. (2008)
Thamnocephalus platyrus 24-h	Nano ZnO (50-70 nm) Bulk ZnO	LC_{50} = 0.18 mg/L LC_{50} = 0.24 mg/L	Thamnoxkit FT™	
Chronic toxicity – aquatic invertebrates				
There are no data available on chronic toxicity to aquatic invertebrates.				
Acute toxicity - Algae				
There is no reliable study available.				
Acute toxicity - Microorganisms				
Activated sludge taken from a municipal wastewater treatment plant 180 min	NM-110	EC_{20} and EC_{50} > 1000 mg/L EC_{10} = 750 mg/L	OECD 209	BASF SE (2012b)

Finally, the data indicated that the aquatic toxicity of nanoscale ZnO is comparable to ZnO bulk material. With respect to the physical and chemical properties, NM-110, NM-111, NM-112, and NM-113 showed different agglomeration behaviour towards each other and in different media (deionized water, fish media,

seawater, daphnia media). However, this difference in agglomeration behaviour did not cause differences in the aquatic toxicity of nanoscale ZnO and ZnO bulk materials.

Sediment toxicity

An acute standard 10-day sediment toxicity test was conducted according to OSPARCOM1995/ASTM E1367-99 under GLP conditions. Thus, adult Corophium volutator (size range 4-7 mm, n = 20) were exposed to NM-112, NM-113 and ionic zinc (no details on purity). Dosing and exposures were done via water or via sediment. The method used to determine the endpoint is not specified. For all tested substances a concentration-dependent increase in mortality was observed in a similar manner. Acute exposure through the overlying water was 10-fold more toxic than acute exposure through the sediment (Fabrega and Galloway, 2010).

In a sediment toxicity study, the organism Corophium volutator was administered over whole life cycle (100 d) with 0.2, 0.5 and 1 mg/L of NM-112 and the reference materials NM-113 and ionic Zn to investigate the effect on mortality, growth and reproductive endpoints. The study was performed according to OSPARCOM1995/ASTM E 1367-99 and under GLP conditions. The organism was treated in water (7 cm of sieved natural sediment and aerated seawater) and examined after 28, 63 and 100 days. Exposure via water to all forms of zinc in the range of 0.2 – 1 mg/L, delayed growth and an affected reproductive outcome.. Solubility studies suggest that toxicity of NPs was not solely due to Zn2+, the possible uptake of ZnO particles via other routes i.e dietary uptake might impact direct comparison between the exposures..STEM-EDX analysis was used to characterize insoluble zinc precipitates (sphaerites) of high sulfur content, which accumulated in the hepatopancreas following exposures. The elemental composition of the sphaerites did not differ for ZnO NP, Zn2+, and bulk ZnO exposed organisms (Fabrega et al., 2012).

Summary and conclusion

Two sediment toxicity studies were conducted to determine the effect of NM-112 and the reference material NM-113 to Corophium volutator after an exposure period of 10 d and 100 d, respectively. Both, in the 10-d sediment toxicity study as well as in the 100-d sediment toxicity study no no-effect concentrations were derived. Exposure was done via water and in the case of the 10-d study in addition via sediment. The results indicated similar effects induced by NM-112 and NM-113, both in the short-term study and the long-term study and no indication was found that NM-112 was more toxic than the bulk product NM-113.

Terrestrial toxicity

Toxicity to terrestrial plants

The toxicity and uptake of ZnO nanoparticles (particle size 20 nm, purity 99.5%) was studied in *Lolium perenne* under non-GLP/guideline conform conditions (Lin and Xing, 2008). ZnO nanoparticles were characterized by TEM and BET analysis. Phytotoxicity experiment included three treatments; no treatment, treatment with ZnO nanoparticles or $ZnSO_4$ heptahydrate solution, respectively. Seedling growth in both treatments was retarded with shorter roots and shoots compared to the control. In addition the seedling biomass decreased with increasing concentrations. The nominal IC_{50} (12 d) of ZnO nanoparticles was 64 mg/L (corresponding to 51 mg/L Zn), which was in a similar range compared to the IC_{50} value of ionic Zn. Furthermore, shrank morphology of the roots tips (epidermis and rootcap were

broken, cortical cells were highly vacuolated and collapsed). It was also observed that ZnO nanoparticles were able to concentrate in the rhizosphere and enter the root cells. The authors suggested that the phytotoxicity of ZnO nanoparticles could not primarily come from their dissolution.

Lin and Xing (2007) also investigated the effect of ZnO nanoparticles (size: 20 nm, purity > 99.5%) on seed germination and root growth. Seeds were soaked in deionized water, nanoparticle suspension or ionic Zn solution for about 2 h. The results indicated that seed germination of ryegrass and corn was inhibited by ZnO nanoparticles. Additionally, ZnO nanoparticles inhibited root growth of corn and practically terminated root development of the plants used. To test the phytotoxicity of ionic Zn in the suspension of ZnO nanoparticles, their supernatant was used and the Zn^{2+} concentration was determined by using ICP-OES. Equivalent concentrations made from ZnSO4 heptahydrate served as reference. Since no phytotoxicity was observed, the authors assumed that the phytotoxicity of ZnO nanoparticles was not directly from their dissolution in bulk aqueous solutions.

In conclusion, ZnO nanoparticles seemed to lead to retarded growth of terrestrial plants and decreased seed germination. However, the validity of the observed effects are considered questionable as apparently Zn ion effects were observed and the occurrence of agglomerates were not addressed.

Overall Summary on the Ecotoxicological Profile

Originally, the OECD nanomaterials NM-110, NM-111, NM-112, and the bulk product NM-113 should be compared in terms of their ecotoxicological profile. Frequently, nanomaterials were only assessed individually for a specific endpoint, so that a comparison of the nanomaterials is limited. Furthermore, also non-OECD nanomaterials (uncoated nanoscale ZnO, ZnO bulk) were investigated, e.g. for acute toxicity to fish.

Almost identical acute toxicity to zebrafish embryos of non-OECD NM (uncoated nanoscale and ZnO/bulk) was observed. The 96-LC_{50} of uncoated nanoscale ZnO and ZnO/bulk were 1.793 mg/L and 1.550 mg/L, respectively (based on mortality rate). The 84-h EC_{50} values were 2.065 mg/L for uncoated nanoscale ZnO and 2.066 mg/L for ZnO/bulk (based on hatching rate). Thus no indications were seen, that uncoated nanoscale ZnO is more toxic than ZnO/bulk.

For the OECD NM the following acute toxicity results to aquatic invertebrates were determined:

NM-112: 48-h LC_{50} = 1.55 mg/L (based on mortality; *Daphnia magna*)

NM-113: 48-h LC_{50} = 3.32 mg/L (based on mortality; *Daphnia magna*)

NM-110: 48-h EC_{50} = 7.5 mg/L (based on mobility; *Daphnia magna*)

NM-111: 48-h EC_{50} = 1.1 mg/L (based on mobility; *Daphnia magna*)

Non-nanoscale ZnO (comparable to NM-113): 48-h EC_{50} = 1.0 mg/L (based on mobility; *Daphnia magna*)

In conclusion, the acute toxicity studies to fish and aquatic invertebrates revealed that nanoscale ZnO is comparable to ZnO bulk.

Concerning the long-term toxicity to fish, the NOEC was ≥ 540 µg/L and the LOEC was > 540 µg/L after 32 days post hatch for NM-110. There are no NOEC or LOEC values indicated for the reference material NM-113 and thus no comparison can be made.

The EC_{50} and EC_{20} values, determined in a 180-min static test were greater than 1000 mg/L. The EC_{10} value was 750 mg/L for NM-110. The inhibition of the degradation activity of activated sludge is not expected when introduced to biological treatment plants in appropriate low concentrations as the EC_{20} value is greater than 100 mg/L. NM-110 was tested separately and thus no comparison with ZnO bulk is possible.

Toxicity to the sediment living organism *Corophium volutator* was comparable for NM-112 and NM-113, both in the short-term and long-term study. It has to be considered that the organism was predominantly exposed via water. Solubility studies suggest that toxicity of NPs was not solely due to Zn^{2+}, the possible uptake of ZnO particles via other routes i.e dietary uptake might impact direct comparison between the exposures. When tested comparatively, the effect was more pronounced in the case of exposure via water instead via sediment. With respect to the physical and chemical properties, NM-110, NM-111, NM-112, and NM-113 showed different agglomeration behaviour towards each other and in different media (deionized water, fish media, seawater, daphnia media). However, this difference in agglomeration behaviour did not cause difference between the toxicity of nanoscale ZnO and ZnO bulk.

Table 29 shows the relevant endpoints in which nanoscale ZnO was tested comparative to ZnO bulk.

Table 29: Summary of relevant and reliable endpoints to aquatic toxicity and sediment toxicity

Organism/ Test duration	Test material	Results	Remarks	Reference
Acute toxicity - Fish				
Zebra fish (*Danio rerio*) 96-h	Uncoated nanoscale	96-h LC_{50}: 1.793 mg/mL (based on mortality) 84-h EC_{50}: 2.065 mg/L (based on hatching rate)	bioassay according to Schulte & Nagel (1994)	Zhu et al. (2008)
	ZnO/bulk	96-h LC50: 1.550 mg/mL (based on mortality) 84-h EC50: 2.066 mg/L (based on hatching rate)		
Acute toxicity – Aquatic invertebrates				
Daphnia magna	NM-112	LC_{50} = 1.55 mg/L	modified OECD 202	Fabrega and Galloway, University of Exeter (2010)
	NM-113	LC_{50} = 3.32 mg/L		

Organism/ Test duration	Test material	Results	Remarks	Reference
48-h				
Daphnia magna	NM-110	EC_{50} = 7.5 mg/L	OECD 202	Wiench et al. (2009)
	NM-111	EC_{50} = 1.1 mg/L		
48-h	Non-nanoscale ZnO < 1µm	EC_{50} = 1.0 mg/L		
Daphnia magna and	Nano ZnO (50-70 nm)	LC_{50} = 3.2 mg/L	Daphtoxkit F^{TM} magna	Heinlaan et al. (2008)
48-h	Bulk ZnO	LC_{50} = 8.8 mg/L		
Thamnocephalus platyrus	Nano ZnO (50-70 nm)	LC_{50} = 0.18 mg/L	Thamnoxkit FT^{M}	
24-h	Bulk ZnO	LC_{50} = 0.24 mg/L		
Sediment toxicity				
Corophium volutator	NM-112 NM-113	Equal toxicity of nanoscale ZnO compared to ZnO bulk	According to OSPARCOM 1995/ASTM E1367-99	Fabrega and Galloway (2010)
10-d				
100-d	NM-112 NM-113			Fabrega et al. (2011)

Finally, when comparatively tested with ZnO bulk, nanoscale ZnO materials revealed an almost identical toxicity to aquatic and sediment organisms, respectively.

Environmental Fate and Pathways of Zinc Oxide (ZnO) Nanomaterials (NM)

Stability

There are no data available on stability in water.

Biodegradation

There are no data available on biodegradation.

Bioaccumulation

There are no reliable data on bioaccumulation.

Transport and distribution

Adsorption / desorption

The retention of uncoated non-nanoscale NM-110, coated nanoscale NM-111, and uncoated nanoscale NM-112 was examined in five soils with varying physical and chemical characteristics (CSIRO, 2012). The retention values (K_r) for all test items in soils were determined using the procedure by Cornelis et al. (2010). In addition, the solid-liquid partitioning (K_d) values for bulk ZnO (NM-113), soluble Zn, and geogenic Zn in soils were determined but only provided for NM-113 and soluble Zn. The last one was used for the calculation of the K_r values. The K_r value is expressed as follow:

$K_r = M_{solid}/M_{NP}$ x L/S (Lkg^{-1}) M_{NP}: small aggregates that pass 0.45 µm membrane filter

M_{solid}: manufactured NPs which aggregate or deposit on soil mineral that do not pass 0.45 µm membrane filter

The K_d values of bulk ZnO (NM-113) and soluble Zn compared to the K_r values of NM-110, NM-111, and NM-112 were in the same order of magnitude. The highest K_r and K_d values for all test items were observed in the "Bute" soil.

Table 30: Partition coefficient (K_d) values for bulk ZnO (NM-113) and soluble Zn

Soils	Bulk ZnO	Soluble Zn
	K_d (L/kg)	**K_d (L/kg)**
Mt Compass	2.9 ± 0.06	2.3 ± 0.04
Ingham	2.3 ± 0.06	1.8 ± 0.04
Emerald Black	3.3 ± 0.04	2.8 ± 0.02
Bute	4.2 ± 0.04	> 5.6
Pt Kenny	3.8 ± 0.04	> 4.3

Table 31: Retention coefficient (K_r) values for NM-110, NM-111, and NM-112

Soils	NM-110	NM-110	NM-111	NM-111	NM-112	NM-112
	K_r (L/kg)	**0.45 µm-1 kDa (%)**	**K_r (L/kg)**	**0.45 µm-1 kDa (%)**	**K_r (L/kg)**	**0.45 µm-1 kDa (%)**
Mt Compass	2.6 ± 0.27	2.9 ± 1.7	2.0 ± 0.08	8.8 ± 1.8	> 3.6	bdl
Ingham	> 4.5	bdl	2.4 ± 0.04	2.5 ± 0.4	> 3.8	bdl

Soils	**NM-110**	**NM-110**	**NM-111**	**NM-111**	**NM-112**	**NM-112**
	K_r (L/kg)	**0.45 µm-1 kDa (%)**	**K_r (L/kg)**	**0.45 µm-1 kDa (%)**	**K_r (L/kg)**	**0.45 µm-1 kDa (%)**
Emerald Black	2.4 ± 0.03	3.8 ± 0.2	2.5 ± 0.22	2.9 ± 1.6	> 3.6	bdl
Bute	> 4.5	bdl	> 3.9	bdl	> 3.4	bdl
Pt Kenny	2.9 ± 0.22	1.4 ± 0.6	> 3.9	bdl	> 3.8	bdl

bdl = below detectable limits

Summary and conclusion

NM-110, NM-111 as well as NM-112 show a similar adsorption/desorption behaviour in different soils.

Thus, there is no different adsorption/desorption behaviour between coated nanoscale and uncoated nanoscale ZnO.

Toxicological Information on Zinc Oxide (ZnO) Nanomaterials (NM)

The nanomaterials NM-110, NM-111, NM-112 as well as non-nanoscale ZnO (corresponding to NM-113) were tested to investigate its toxicological profile.

Toxicokinetics

In vitro and *in vivo* dermal absorption studies were conducted with NM-110 and NM-111. In addition, two *in vivo* inhalation studies investigated also toxicokinetics.

Studies in Animals

In vitro Studies

Dermal

In an *in vitro* dermal absorption study according to OECD 428 under GLP conditions, dermatomed pig skin mounted on Franz-type diffusion cells was treated with nominal doses of 4 mg/cm^2 of a 10% oil/water formulation of NM-110 (corresponding to approx. 400 µg/cm^2 ZnO or 320 µg/cm^2 Zn^{2+}) for 24 hours. The pig skin used as diffusion barrier between the donor compartment of a diffusion cell and the receptor compartment filled with the receptor medium. At the end of exposure, the test substance was removed from skin preparations by tape stripping and was also recovered from all other relevant compartment of each diffusion cell (considered as non-absorbed). Fractions present in the remaining skin after tape stripping and receptor chamber fraction are considered as recovery. Zinc analyses were carried out by using the Flame Atomic Absorption Spectrometry. The results indicated that no Zn^{2+} from the NM-110 containing formulation penetrated through the skin of domestic pigs under the conditions of this study (BASF SE, 2005). In addition, these results show that microfine ZnO particles are not able to penetrate the porcine dermatomed skin preparations.

The aim of another study (non-GLP conform) was to determine whether porcine skin damaged by moderate UVB radiation enhanced the penetration of 5% NM-111 or 5 % NM-110 present in sunscreen oil/water formulation (see cross reference to the *in vivo* study). The penetration of the nanoparticles was investigated *in vitro* through dermatomed porcine skin in flow-through diffusion cells, 24 h after *in vivo* UVB exposure. The perfusate was collected every 2 h for the first 12 h, then every 4 h up to 24 h. Analysis was performed by applying light microscopy, scanning electron microscopy, transmission electron microscopy (TEM) as well as Time-of-Flight secondary mass spectrometry (TOF-SIMS) and Inductively coupled plasma mass spectrometry (ICP-MS). In summary, UVB-damaged skin did not enhance the penetration of the nanoparticles in the provided sunscreen formulations. The nanoparticles remained on the surface and within upper stratum corneum layers. In UVB unexposed skin, NM-111 and NM-110 remained on the surface. While Zn was found to penetrate into the stratum corneum by TEM and into the epidermis by TOF-SIMS, there was no definitive evidence by these optical methods that the nanoparticles penetrated into the perfusate (BASF SE, 2009a; Monteiro et al., 2011).

In vivo Studies

Dermal

An *in vivo* dermal absorption GLP-conform study in rats was conducted according to OECD 427 using radiolabelled [^{65}Zn] NM-111 (purity 98%). Two mg/cm^2 of the test item (in corn oil) were administrated to the prepared skin of each animal and the application site was covered by non-occlusive gauze which did not contact the skin due to a spacer. Group 1 was killed directly after the 6 hours exposure period, group 2 and 3 after a recover period of 18 and 66 hours. No relevant radioactivity was found in faeces, urine, cage wash, and organ or tissue samples. In conclusion, NM-111 was not absorbed through the skin after dermal application in rats during the study (CEFIC, 2013a).

Additionally, the impact of 5% NM-111 or 5% NM-110 present in sunscreen oil/water formulation was investigated after exposure to porcine skin damaged by moderate UVB radiation *in vivo*. The non-GLP study followed no guideline. The UVB exposed sites of pigs were treated with the formulation for 48 h. Analysis was performed by applying light microscopy, scanning electron microscopy, transmission electron microscopy (TEM) as well as Time-of-Flight secondary mass spectrometry (TOF-SIMS) and Inductively Coupled Plasma Mass Spectrometry (ICP-MS). Comparable effects were observed as shown in the *in vitro* study. Thus, no transdermal absorption was detected for 5% NM-111 and 5% NM-110 in sunscreen formulations (BASF SE, 2009; Monteiro et al., 2011).

Osmond-Mc Leod (2014) investigated the skin absorption and organ distribution of a traceable form of Zn (^{68}Zn) from ^{68}ZnO nano-sized and larger particles (bulk) in sunscreens in virgin and pregnant immune-competent hairless mice under non GLP/guideline conform conditions. 0.1 g per application was applied to the back and sides of each mouse (average surface area 50 cm^2), corresponding to a dose of 2 mg/cm^2 for 4 days. Controls received topical applications of the sunscreen formulation only or no treatment. Major organs (brain, liver, spleen, kidneys, lung, heart and from pregnant mice, the uterine tissue and fetal liver were also taken) were assessed for changes in ^{68}Zn/^{64}Zn ratios, ^{68}Zn tracer and total Zn concentrations. Short-term biological impact was assessed by measuring levels of serum amyloid A in blood, and by performing whole genome transcriptional profiling on livers from each group. The authors suggested that ZnO particles in sunscreen did not elicit an adverse biological response in mice. Mice receiving topical applications of ^{68}ZnO (nano-sized and larger particles) showed elevated concentrations of ^{68}Zn in internal organs, as well as in fetal livers from treated dams, compared with controls. Furthermore, concentrations of ^{68}Zn in organs of virgin mice treated with sunscreen containing ^{68}ZnO nanoparticles were found to be significantly higher than in mice treated with sunscreen containing larger ^{68}ZnO particles. However, the total Zn concentration in organs in ZnO-treated mice was not changed. In conclusion, ^{68}Zn absorption was higher in mice receiving topical applications of ^{68}ZnO nano-sized compared to ^{68}ZnO bulk. It cannot be concluded whether soluble ^{68}Zn or ^{68}ZnO particles were measured. However, it cannot be concluded whether enriched 68Zn has been detached and to which extend and was absorbed as ZnO particles or soluble Zn. It should be considered that ions might detach as a part of the zinc and indicates positive false results. Furthermore, it has to be considered that skin penetration in hairless mice is generally higher compared to humans.

Inhalation

Toxicokinetics according to OECD 417 under non-GLP conditions were examined as part of Repeated Dose Inhalation Toxicity Studies (cross-reference to 0). In the 14-day-inhalation-study performed by CEFIC 2013b, the Zn content was analyzed by ICP-MS in the lung-associated lymph nodes (LALN),

brain, kidneys, liver, lung and in blood and urine in 5 rats per group. Rats were exposed for 2 weeks, 5 consecutive days per week, 6 hours per day to NM-111 (0.5, 2 and 8 mg/m3), and the reference materials NM-110 (8 mg/m^3) and NM-113 (8 mg/m^3), respectively. One day after end of exposure, in the high dose group of NM-111 the absolute Zn content was slightly increased (statistically significant) to 365% in the lung as compared to the clean air control group. In all other organs the Zn levels were very close to the control values. The deposited mass of NM-111 in the 10-day exposure period was approximately 290 µg/lung. The analytical results demonstrated a practically complete dissolution of the retained test item. After 14-day recovery, only incidental findings were observed. Overall, no relevant amounts of increased NM-111 were detected in anybody compartment demonstrating, the rapid elimination. The absolute Zn content following exposure to NM-110 and NM-113 in lung were in the same order but not significantly increased. The corresponding dose range finding study (5 days exposure) also investigated the toxicokinetic behaviour of NM-111 (CEFIC, 2009). Only the high dose group (8 mg/m^3 NM-111) revealed slightly increased absolute zinc contents in liver, kidney, and brain one day after the end of the exposure period, while urine and blood were not affected.

Zn analysis was also performed as additional parameter according to OECD 417 in a 90-day-inhalation study under GLP conditions (cross reference to 0) (CEFIC, 2011a). The absolute Zn content was examined in organs, blood, and urine on day 1 and 29 after end of exposure. On the first day post exposure the Zn content in lungs of animals treated with the NM-111 high dose (4.5 mg/m^3) was increased to 180% compared to the control. The deposited mass of the test item in the 90 days exposure period was approx. 2000 µg/lung. The analytical results demonstrated a practically complete dissolution of the retained test item. No significantly increased amount of the test item was detected in any other body compartment.

Intravenous

A modified GLP-conform OECD 407 study with intravenous injection was performed to compare equimolar concentrations of NM-111 (purity > 97.1% ZnO), NM-110 (purity: no details), ZnO pigment (purity > 99%, comparable to NM-113) as well as $ZnSO_4$ heptahydrate (purity: 100%) (COLIPA AISBL, 2009). The complete study consisted of a 28-day toxicity part in male and female rats (subset 0) as well as an organ distribution part in male rats after 1 and 29 days after dosing (subset 1 and 2). The test items were administrated once (unless otherwise indicated) to Wistar rats per test group by intravenous administration as follows:

Subset 0 (treatment on day 0 with 28-day post-exposure period): 1 and 5 mg/kg bw NM-111 and NM-110 or 5 mg/kg bw ZnO pigment; repeated i.v. administration 4.4 mg/kg bw $ZnSO_4$ heptahydrate on day 0, 7, 14 and 21

Subset 1 (single administration 1 day prior to necropsy): 1 and 5 mg/kg bw NM-111 and NM-110; 5 mg/kg bw ZnO pigment; 17.6 mg/kg bw $ZnSO_4$ heptahydrate.

Subset 2: like subset 0 followed by perfusion fixation

The intravenous application route represents a worst-case scenario and was selected to guarantee systemic bioavailability of 100%.

No test substance-related findings were observed in animals of subset 0 or 2. Very mild deviations in the differential blood cell count (monocyte, large unstained cells) and few clinical chemistry parameters, indicative for a minimal impairment of liver function (NM-110, NM-111 and ZnO pigment (comparable to NM-113)) or of kidney function in addition ($ZnSO_4$ heptahydrate) were observed 1 day after intravenous injection of 5 mg/kg bw NM-110, NM-111 and ZnO pigment (comparable to NM-113) or an equimolar $ZnSO_4$ heptahydrate dose. At 1 mg/kg bw, no biological relevant effect was observed. Among the sensitive markers of acute phase reactions heptaglobulin was increased, while α2-macroglobulin was not affected. Finally, the comparative screening showed only minor and in any case transient effects without toxicological relevance. There was no biologically relevant difference in the injected form of ZnO, especially no enhancement of the observed effects due to the injection of nanoscale material. In any case, 4 weeks after treatment there was virtually no difference in comparison to the respective control group, irrespectively of the injected dose level and the usage of ZnO as nanoparticles, as pigment or as $ZnSO_4$.

Studies in Humans

In vitro Studies

The distribution of topically applied nano-sized ZnO (mean primary particle size: 26–30 nm with preservatives of phenoxyethanol (0.3% w/w) and hydroxybenzoates (0.3% w/w)) in excised human skin after application of a commercial sunscreen was examined in a non-GLP/guideline conform study. Multiphoton microscopy (MPM) imaging with a combination of scanning electron microscopy (SEM) and an energy-dispersive X-ray (EDX) technique were used for measurement. Abdominal or breast skin obtained following plastic surgery was used. The cross-sectional imaging showed no evidence of nano-sized ZnO penetration into the cells or extracellular space (Zvyagin et al. 2008).

Human epidermal skin penetration of a novel, transparent, nanoparticulate zinc oxide sunscreen formulation (ZnO dispersion of 60% siliconate coated ZnO in caprylic capric triglyceride and O/W emulsion sunscreen with 20% ZnO siliconate coated ZnO in caprylic capric triglyceride, respectively) was determined using Franz-type diffusion cells under non GLP/guideline conform conditions. After 24-hour exposure, electron microscopy was used to verify the location of nanoparticles in exposed membranes. Less than 0.03% of the applied zinc content penetrated the epidermis (not significantly more than the zinc detected in receptor phase following application of a placebo formulation). No particles could be detected in the lower stratum corneum or viable epidermis by electron microscopy, suggesting that minimal nanoparticle penetration occurs through the human epidermis (Cross et al, 2007).

In vivo Studies

Gulson et al. (2010) examined dermal penetration of Zn from ZnO nanoparticles in sunscreen applied to human skin under non-GLP/guideline conform conditions. In total 20 volunteers were examined. Each group was exposed to 2 mg/cm^2 nano sunscreen (20% wt/wt ZnO particles (mean size 19 nm) enriched with ^{68}Zn in oil/water formulation) and bulk sunscreen (20% wt/wt ZnO particles (mean size 110 nm) enriched with ^{68}Zn in oil/water formulation), respectively. The subjects were treated for 5 days (twice

daily) and after each application a minimum of 30 min UV exposure followed. Venous blood and urine samples were collected 8 days before exposure, twice daily during the trial, and 6 days post-exposure. It was shown that the majority of applied ^{68}Zn was not absorbed. Only small increases in levels of tracer ^{68}Zn in blood and urine samples were noted. The amount of ^{68}Zn tracer detected in blood post trial represented less than 0.0001% of the applied dose. Levels of ^{68}Zn in blood and urine samples from females receiving the nano sunscreen appeared to be higher for male bulk, male nano, and female bulk groups. However, it has to be considered that one subject who had an adverse reaction to the sunscreen, and application was included in the analyses with damaged skin. However, It cannot be concluded whether enriched 68Zn has been detached and to which extend and was absorbed as ZnO particles or soluble Zn. It should be considered that ions might detach as a part of the zinc and indicates positive false results.

Subsequently, Gulson et al. (2012) conducted a pilot study (non-GLP/guideline conform) to examine the dermal penetration of Zn from ZnO nanoparticles in sunscreen in only 3 human volunteers under conditions of limited UV exposure and compared the results with those of the outdoor trial (Gulson et al. 2010). Nanoparticles (size 30 nm) of a stable isotope (52% ^{68}Zn enrichment) were incorporated into a sunscreen and applied to the backs of the volunteer twice daily for 5 days. Increase of ^{68}Zn in blood were recorded following 5 days application with the highest amount at 14 days after the first application. Variable amounts of the ^{68}Zn tracer were observed in urine; and the amounts of extra Zn added to blood were small and indicate very low levels of absorption (minimal estimate <0.01% of the applied dose) through the skin. The authors suggested that small amounts of Zn from ZnO nanoparticles in sunscreen were absorbed through the skin in both trials. Irrespectively different sunscreen formulations and different UV exposure scenarios were used. However, it cannot be concluded whether enriched ^{68}Zn has been detached and to which extend and was absorbed as ZnO particles or soluble Zn. It should be considered that ions might detach as a part of the zinc and indicates positive false results.

Summary and conclusion

Both, reliable and conclusive *in vitro* and *in vivo* studies showed that neither NM-110 nor NM-111 ZnO was absorbed through the skin. Thus, the uncoated ZnO (NM-110) does not behave different than the coated ZnO (NM-111) and no high bioavailability has to be expected after skin contact. The *in vivo* inhalation studies revealed that exposure to NM-111 increased the Zn content in the lung. When tested in comparison with NM-113 and NM-110 a similar behaviour was observed.

Table 32: Reliable and conclusive toxicokinetics studies

Method, OECD	Test substance, Concentration, Results	Reference
Dermal		
In vitro		
dermatomed pig skin, OECD 428	4 mg/cm^2 NM-110 (10% in oil/water formulation): did not penetrate through the skin	BASF SE (2005)
Porcine skin damaged by moderate	NM-110 and NM-111 respectively (5% in	BASF SE (2009a) and

Method, OECD	Test substance, Concentration, Results	Reference
Dermal		
In vitro		
UVB radiation, No guideline	oil/water formulation): did not penetrate in perfusate	Monteiro et al. (2011)
In vivo		
Rats, non-occlusive gauze, 6, 18 or 66 h exposure, OECD 427	2 mg/cm^2 NM-111 (in corn oil): not absorbed	CEFIC (2013a)
UVB exposed sites of pigs, 48 h exposure, No guideline	NM-110 and NM-111 respectively (5% in oil/water formulation): no transdermal absorption	BASF SE (2009a) and Monteiro et al. (2011)
Inhalation		
In vivo		
Rats, 2 weeks, 5 d/w, 6 h/d OECD 417	0.5, 2 and 8 mg/m^3 NM-111 8 mg/m^3 NM-110 and NM-113 NM-111 (8 mg/m^3): Absolute Zn content in lung was slight increased on day 1 post exposure	CEFIC (2013b) Part of 14-day-inhalation-study
Rats 3 months, 5 d/w, 6 h/d OECD 417	4 mg/m^3 NM-111 Zn content in lung was increased to 180% on day 1 post exposure	CEFIC (2011a) Part of 90-day-inhalation-study
Intravenous		
In vivo		
Rats Single administration (intravenous), different post-exposure period Modified OECD 407	1, 5 mg/kg bw NM-111 and NM-110 5 mg/kg bw ZnO pigment (comparable to NM-113) No test substance-related findings	COLIPA (2009)

Acute toxicity

The acute toxicity of the OECD NM-111 and of the non-OECD nanoscaled ZnO (particle size: 20 nm) as well as submicroscaled ZnO (particle size: 120 nm) has been characterized from dermal and oral studies in rats and mice.

Studies in Animals

Inhalation

There are no data available on acute inhalation toxicity.

Dermal

The dermal acute toxicity of NM-111 was tested in a GLP-conform study according to OECD 402 (CEFIC, 2010a).

2000 mg/kg bw of NM-111 were administered for 24 hours as pasty formulation in corn oil (0.5 mg test item in 400 µL corn oil) to the shaved and defatted back of 5 female and 5 male rats. A detailed test item preparation was not indicated. The animals were covered in a semi-occlusive manner with a gauze dressing which was fixed using a non-irritating tape. After the end of the 24-hour exposure period the test item paste was recovered as effectively as possible using water and the animals were observed for 14 days.

During the present study no mortality occurred and there were no indications of systemic toxicity, no effects regarding the body weight and neither clinical signs nor pathological findings were observed. The LD_{50} was therefore estimated to be > 2000 mg/kg bw in rats.

Oral

Wang et al. (2008) treated 5 mice per sex and dose orally by gavage with 1000, 2000, 3000, 4000 and 5000 mg/kg bw of non-OECD nanoscaled ZnO powder (particle size: 20 nm) and non-OECD submicroscaled ZnO powder (particle size: 120 nm), respectively. The study was performed according to guideline but under non-GLP conditions. According to the particle size, nanoscaled ZnO powder is comparable to OECD NM-112 and submicroscaled ZnO powder is comparable to OECD NM-113. After the 14-days observation period the oral LD_{50} of 20 nm ZnO was estimated to be > 5000 mg/kg bw while the LD_{50} of 120 nm ZnO was > 2000 and < 5000 mg/kg bw in mice.

Summary and conclusion

The dermal acute LD_{50} value of NM-111 was determined according to OECD 402 in rats under GLP conditions. The LD_{50} value was > 2000 mg/kg bw (CEFIC, 2010a).

Oral acute toxicity study was performed with non-OECD materials in studies comparable to OECD 401. The LD_{50} value of nanoscaled ZnO powder (20 nm) was > 5000 mg/kg bw while the LD_{50} of 120 nm ZnO was > 2000 and < 5000 mg/kg bw in male and female mice (Wang et al., 2008).

The acute toxicity studies indicated that nano ZnO is comparable toxic than bulk ZnO. Especially the acute dermal toxicity results fit to skin penetration data.

Table 33: Relevant acute toxicity studies

Method, species/strain, sex	Results	Reference
Dermal		
Acute dermal toxicity rat (Wistar) male/female Coverage: semi-occlusive Vehicle: corn oil	LD50: > 2000 mg/kg bw (male/female) based on: NM-111 (no mortality occurred)	CEFIC (2010a)
Oral		
Acute oral toxicity mouse (CD-ICR) male/female administration: gavage	LD_{50}: > 5000 mg/kg bw (male/female) (20 nm ZnO) LD_{50}: > 2000 — < 5000 mg/kg bw (male/female) (120 nm ZnO)	Wang, B. et al. (2008)

Irritation/ corrosion

Skin Irritation

In vitro Studies

NM-111 (purity 98%) was tested in an *in vitro* skin corrosion test according to OECD 431 applying a reconstructed human skin model under GLP conditions. Two EpiDerm tissues were treated for 3 minutes and 1 hour, respectively, with the test item (25 mg/25 µL water). However, it has to be considered that water has some limitations as solvent for coated NM (for detailed information please refers to annex I, section 7.3.1). Water served as negative control and 8 N KOH as positive control. At the end of the exposure period the cell viabilities of the treated tissues were measured using MTT test calculated as percent relative to the negative control. The test substance is considered to be non-corrosive to skin as the cell viability was greater than 50% after 3 minutes of exposure and greater than 15% after 1 hour of exposure. The positive control was considered to be corrosive to skin as expected (CEFIC, 2010b).

Eye Irritation

In vitro Studies

The potential of NM-110 (purity 99%) to cause serious damage to the eyes was estimated according to OECD 437 by using a non-GLP conform Bovine Corneal Opacity and Permeability Test (BCOP Test) (BASF SE, 2011a). Therefore, 20% (w/v) test-substance preparation (non-surfactant) was applied directly to the epithelial surface of the cornea using a pipette (open chamber method). It has to be noted that no detailed description of test item preparation was indicated. Controls were concurrently applied into the anterior chamber with highly deionized water or with a 20% (w/v) solution of imidazole (positive control) using a pipette. The corneas were incubated at about 32°C for approximately 4 hours (non-surfactant-solids). After removal of the substance, corneal opacity and permeability were measured. Based on the

results, it was concluded that NM-110 does not cause serious eye damage in the BCOP test under the test conditions chosen.

The potential of NM-110 (purity > 99%) to cause ocular irritation was also assessed by a single topical application of 50 µL bulk volume (about 12 mg) of moistened test substance to a reconstructed three dimensional human cornea model (EpiOcular^{TM}) for an exposure period of 90 min under non-GLP conditions (BASF SE, 2011b). The study was performed according the methods described in the publication of MatTek Corporation (2010) and Harbell et al. (2009). Tissue destruction was determined by measuring the metabolic activity of the tissue after exposure/post-incubation using a colorimetric test (MTT test). The mean tissue viability of NM-110 was determined to be 98% and thus the test substance was not an eye irritant in the EpiOcular^{TM} test under the test conditions chosen.

Respiratory Tract Irritation

Studies in Animals

There are no data available on the respiratory irritation in animals.

Studies in Humans

There are no data available on the respiratory tract irritation in humans.

Summary and conclusion

NM-111 is considered to be non-corrosive to skin based on the results of the *in vitro* skin corrosion test according to OECD 431.

NM-110 does not cause serious eye damage in the BCOP test *in vitro* under the test conditions chosen. In addition, the test substance was not an eye irritant *in vitro* in the EpiOcular^{TM} test.

It can be concluded, that uncoated nano ZnO (NM-110) and coated nano ZnO (NM-111) revealed no high skin or eye damaging potential.

Sensitisation

There are no data available on sensitisation.

Repeated Dose Toxicity

Studies in Animals

Inhalation

A 90-day inhalation study was conducted in rats using nose-only exposure according to OECD 413 under GLP conditions (CEFIC, 2011a). Additional endpoints (bronchoalveolar lavage (BAL), cell proliferation, electron microscopy analysis, and toxicokinetics (cross-reference to 0) were included to investigate potentially nano-specific aspects of toxicity. The animals were treated with 0.3, 1.5 and 4.5 mg/m3 coated nanoscaled ZnO (NM-111, purity 98%), respectively, as well as 4.5 mg/m3 non-coated microscaled ZnO

(NM-113, no details on purity) for 3 months, 5 consecutive days per week (6 h/d). Fresh air treated animals served as concurrent control. The absolute lung wet weights of the NM-113 treated animals was significantly increased. Histopathological examination and changes in BAL parameters revealed findings restricted to the respiratory tract indicating inflammatory reactions of the lung. These effects were comparable for both of the tested ZnO particles, mainly restricted to the high dose (4.5 mg/m3) treated animals, not statistically significant for the low dose treated group, and fully reversible or reduced in severity after the recovery period. The retained material was completely solved and eliminated rapidly since no increased Zn contents were detected in anybody compartment after the post-exposure period. Neither NM-111 nor NM-113 induced hyperplastic effects in the lungs. Based on the results of the present study the NOAEC for NM-111 was assessed to be 1.5 mg/m3.

In addition, 12.5 mg/m3 ZnO powder (Sigma-Aldrich, corresponding to NM-113, purity 99.9%) and 0.5, 2.5, and 12.5 mg/m3 (target concentration) coated nanoscaled ZnO (NM-111, purity 97.3% ZnO,) were tested in a 5-days nose-only lung toxicity study similar to OECD 412 under non-GLP conditions (Ma-Hock et al. 2008, BASF SE 2010). 17 male rats per group were treated 6 h per day for 5 consecutive days followed by a 3 weeks observation time. NM-111 caused local inflammations in the lungs of the rats, indicated by changes in several parameters in the bronchoalveolar lavage fluid (BALF) and histological examinations. Secondary to the effect in the lung, activation of the draining lymph nodes and minimal to moderate necrosis of the olfactory epithelium was noted. These effects were in a concentration-related manner and reversible within the recovery period. Only a multifocal increase in alveolar macrophages was still present at the end of the recovery period. Similar effects were also observed in the animals exposed to ZnO powder. At the low concentration of 0.5 mg/m3 NM-111, increased levels of a few mediators in the BALF and serum were determined. Moreover minimal multifocal necrosis of the olfactory epithelium was noted in the nasal cavity in one animal. Therefore, the lowest target concentration of 0.5 mg/m³ was considered to be the Low Observed Adverse Effect Concentration (LOAEC).

Furthermore, a non-GLP conform dose range finding study (CEFIC, 2009) was conducted, where 5 male Wistar rats per dose group were exposed for 5 consecutive days and 6 hours per day with 0, 0.5, 2 and 8 mg/m3 of coated nanoscaled ZnO (NM-111, purity 98%) by nose-only-inhalation. The study was conducted according to OECD 412 in due consideration of animal treatment for only 5 consecutive days and a reduced spectrum of investigated endpoints. The lung weight/body weight ratio was increased in the low and high dose group. Histopathological findings concerning nasal and paranasal activities, lungs and lung-associated lymph nodes were also observed. Additionally, toxicokinetics investigations were conducted (cross-reference to 0).

A GLP-conform study according to OECD 412 (Repeated Dose Inhalation Toxicity: 28/14-Day) was conducted. 45 male Wistar rats per dose group were treated with 0.5, 2, and 8 mg/m3 NM-111 (purity 98%) and with 8 mg/m3 of the reference items NM-110 and NM-113 for 14 days on 5 consecutive days per weeks for 6 hours per day (CEFIC, 2013b). The concentrations based on the dose range finding study mentioned above (CEFIC, 2009). No indication of systemic toxicity was observed. Test substance related histopathological effects were detected especially in the high dose group and were restricted to the respiratory tract indicating reactions in the lung. These effects were comparable for all of the three test items and fully reversible within 14 days. This study was combined with non-GLP conform genotoxicity tests such as Mammalian Erythrocyte Micronucleus Test, hOGG1-modified Comet Assay and

immunohistochemical detection of oxidative DNA damage (cross reference to 0) and a non-GLP toxicokinetic study (cross reference to 0). Furthermore, a bronchoalveolar lavage fluid (BALF) analysis was conducted, which revealed statistically significant increases of polymorphonuclear neutrophils and lactic dehydrogenase, ß-glucuronidase and total protein levels and also an increase of absolute numbers of macrophages in the high dose groups of NM-111, NM-110 and NM-113 1 day after end of exposure. However, all these effects were reversible and had returned to control levels at the 14-day post-exposure sacrifice date. With regard to oxidative stress, the secretion of ROI was enhanced in the 0.5 and 2 mg/m^3 NM-111 treated animals as compared to clean air controls. An increased concentration of the stimulatory cytokines CINC-1, tumor necrosis factor- α, interleukin-6 and the more deregulating mediator transforming growth factor- β (TGF- β) was measured in the NM-111 and NM-113 treated animals. The following table shows significant effects on BAL parameter.

Table 34: BAL parameter

BAL parameter	NM-111 0.5 mg/m^3	NM-111 2 mg/m^3	NM-111 8 mg/m^3	NM-110 8 mg/m^3	NM-113 8 mg/m^3
Neutrophils (PMN)	-	-	↑	↑	↑
Lymphocytes	-	-	-	-	-
LDH/β-Glucuronidase	-	-	↑	↑	↑
Total Protein Day 1	-	-	↑	↑	↑
TNF-α	-	↑	↑	-	↑
IL-6	-	↑	↑	-	-
IL-8 (CINC-1)	-	-	↑	-	-
TGF-β	↑	↑	↑	-	-
↑: increased					

The concentration of the cytokines TNF-α, IL-6, IL-8 and TGF-β was calculated using commercially available ELISA systems. However, it has to be considered that nanoparticles may interfere with ELISA assays (Guidance on information requirements and chemical safety assessment, Appendix R7-1, Chapter R7a, Nanomaterials) and therefore the results have to be treated with caution.

Under the conditions of this test an NOAEL of 2 mg/m^3 for NM-111 was derived (decisive endpoints: BAL: Cellular and enzymatic response; histopathology: bronchiolo-alveolar hyperplasia and mononuclear cell infiltration)

Dermal

There is no repeated dose dermal toxicity study available.

Oral

There is no repeated dose oral toxicity study available.

Studies in Humans

There are no repeated dose studies in humans.

Summary and conclusion

NM-111 and NM-113 were tested in repeated dose inhalation studies with different durations: 90 days (CEFIC, 2011a), 5 days (Ma-Hock et al. 2008, BASF SE 2010) and 14 days (CEFIC, 2013b). Both test items caused comparable and reversible histopathological findings restricted to the respiratory tract, clearly related to the inhalation of particles rather than to the chemical entity. In addition, NM-110 was also investigated in the 14-day inhalation study (CEFIC, 2013b). The effects were comparable to NM-111 and NM-113. The NOAEC for NM-111 was assessed to be 1.5 mg/m^3 and 2.0 mg/m^3 based on the results of the 90-d study and 14-d study, respectively. The LOAEC of NM-111 is 0.5 mg/m^3 determined from the 5-d study. There are no indications, that the coated nano ZnO (NM-111) was more toxic than the uncoated nano ZnO (NM-110) or the bulk product (NM-113).

The 5-day dose range finding study (CEFIC, 2009) supports the results from the 90-d, 5-d and 14-d studies and revealed histopathological findings restricted to the respiratory tract.

Table 35: Relevant repeated dose toxicity studies

Species, strain, number, sex/group	Duration, concentration	NOAEC, findings, remarks	Reference
Inhalation			
rat (Wistar) male 65 animals per dose group	Subchronic (90 days), 5 d/w, 6 h/d inhalation: aerosol (nose only) 0.3, 1.5 and 4.5 mg/m^3 (target aerosol concentration of **NM-111**) 4.5 mg/m^3 (target aerosol concentration of **NM-113)**	Additional endpoints: bronchoalveolar lavage, cell proliferation, electron microscope analysis and toxicokinetics (non-GLP) NOAEC (**NM-111):** 1.5 mg/m³ air (male) based on: test mat. (decisive endpoints: LDH in BAL fluid, histopathology: bronchiolo-alveolar hyperplasia and mononuclear cell infiltration)	CEFIC (2011a)
rat (Wistar) male 17 animals per dose group	5 days (6 h/day), observation period 3 weeks Inhalation: respirable dust	Histopathology restricted to respiratory tract, mediastinal lymph nodes, brain with olfactory bulb	Ma-Hock, L. et al. (2008) BASF SE (2010)

Species, strain, number, sex/group	Duration, concentration	NOAEC, findings, remarks	Reference
Inhalation			
	(nose/head only) 12.5 mg/m^3 (target conc. of ZnO powder, corresponding to **NM-113**) 15.3 ± 1.6 mg/m3 (measured conc. of ZnO powder, corresponding to **NM-113**) 0.5, 2.5 and 12.5 mg/m^3 (target conc. of **NM-111**) 0.55 ± 0.24, 2.76 ± 0.63, and 13.8 ± 2.0 mg/m^3 (measured conc. of **NM-111**)	<u>Additional endpoints:</u> bronchoalveolar lavage no NOAEC identified: (male) (increased levels of some mediators in the BALF and in serum, minimal multifocal necrosis of the olfactory epithelium in one animal) LOAEC: 0.55 mg/m³ air (analytical) (male) (increased levels of some mediators in the BALF and in serum, minimal multifocal necrosis of the olfactory epithelium in one animal)	
rat (Wistar) male 5 animals per dose group	5 d, 6 h/d Inhalation: aerosol (nose only) NM-111: 0.5, 2 and 8 mg/m^3 (target aerosol concentration)	Dose range finding study same doses will be used for subsequent OECD 412 study (CEFIC, 2013b)	CEFIC (2009)
rat (Wistar) male 45 per dose group	2 weeks, 5 d/w, 6 h/d Inhalation (aerosol): nose only 0.5, 2, and 8 mg/m^3 (target aerosol concentration of	<u>Additional endpoints:</u> bronchoalveolar lavage, electron microscopy NOAEC = 2 mg/m^3 decisive endpoints: BAL: Cellular and enzymatic	CEFIC (2013b)

Species, strain, number, sex/group	Duration, concentration	NOAEC, findings, remarks	Reference
Inhalation			
	test item NM-111) 8 mg/m^3 (target aerosol concentration of reference item NM-110) 8 mg/m^3 (target aerosol concentration of reference item NM-113)	response; histopathology: bronchiolo-alveolar hyperplasia and mononuclear cell infiltration	

Mutagenicity

In vitro Studies

NM-113 (purity 80.16%) was tested using the Bacterial Reverse Mutation Assay according to OECD 471 under GLP conditions (BASF SE, 2012a). Standard plate and preincubation tests were conducted in the absence of S9 mix with doses of 20, 100, 500, 2500 and 5000 µg/plate using the S. typhimurium strains TA 1535, TA 100, TA 102, TA 1537 and TA 98. Precipitation of the test substance occurred from about 500 µg/plate and a bacteriotoxic effect was occasionally observed depending on the strain and test conditions from about 2500 µg/plate onward. A relevant increase in the number of his+ revertants was not observed in the standard plate or in the preincubation test in the absence of a metabolizing system. Thus, NM-113 was not mutagenic under the test conditions chosen.

The mutagenic potential of the coated ZnO nanomaterial Z-COTE MAX, which based on NM-111 were investigated by using the Bacterial Reverse Mutation Assay according to OECD 471 under GLP conditions (BASF SE, 2009c). Standard plate and preincubation tests were conducted in the presence and absence of S9 mix with doses of 20, 100, 500, 2500 and 5000 µg/plate using the S. typhimurium strains TA 1535, TA 100, TA 102, TA 1537 and TA 98. Precipitation of the test substance occurred from about 2500 µg/plate onward but no bacteriotoxic effect was observed. A relevant increase in the number of his+ revertants was not observed in the standard plate or in the preincubation test with and without of a metabolizing system. Thus, Z-COTE MAX is not mutagenic under the test conditions chosen. It should be noted that there is evidence that the Ames test is not suitable for the detection of genotoxicity of nanomaterials (Landsiedel et al. 2009, cited in: Guidance on information requirements and chemical safety assessment, Appendix R7-1, Chapter R7a, Nanomaterials).

NM-111 (purity 98% ZnO) was tested using the *In Vitro* Mammalian Cell Gene Mutation Test according to OECD 476 (CEFIC, Fraunhofer ITEM 2011c) in comparison to the reference items NM-110

and NM-113 under GLP conditions. Mouse lymphoma L5178Y/TK$^{\pm}$ cells in suspension culture were treated for 4 hours with different concentrations of NM-111 in the presence or absence of metabolic activation (without S9-mix: 1, 2, 4, 5, and 6 µg/mL; with S9-mix: 2.5, 5, 7.5, and 10 µg/mL). NM-111 induced increases of mutant frequency (MF) in both replicates at 6 µg/mL without S9-mix (relative total growth: 21% compared to vehicle control) and 7.5 µg/mL with S9-mix (relative total growth: 50% compared to vehicle control), and in one replicate at 5 µg/mL without S9-mix (relative total growth: 62% compared to vehicle control). However, significantly increased MF was always linked to cytotoxicity. In the presence of S9-mix relevant increases in MF were obvious for both reference items at 7.5 µg/mL (relative total growth: ≤ 52% compared to vehicle control) but also linked to cytotoxicity. Furthermore, slightly increased turbidity was noted for NM-111 at 10 µg/mL, for NM-110 at 7.5 µg/mL as well as for NM-113 which may influence the conduct of the test. The test results are considered as ambiguous by the author for NM-111, NM-110 as well as for NM-113 as increases in mutant frequency were always linked to cytotoxicity.

NM-111 (purity 98%) was further tested using the *In Vitro* Mammalian Chromosome Aberration Test according to OECD 473 (CEFIC, Fraunhofer ITEM 2010c) in comparison to the reference items NM-110 and NM-113. The assay was performed under GLP conditions. It has to be considered that there is no description for test item preparation. Proliferating V79 cells were treated for 4 hours with different concentrations of NM-111 (1, 3, 5, 10, 12.5, 15, 20, 25, and 50 µg/mL) and the two reference items (3, 10, and 12.5 µg/mL) with and without S9-mix and for 24 hours without S9-mix. After a 4 h exposure period NM-111 caused dose-dependent cytotoxicity while the highest dose decreased the mitotic index (MI) to 44.4% (with S9-mix) and 47% (without S9-mix) of the negative control. There was also a decrease in MI for NM-110 (44.4% at 10 µg/mL) and for NM-113 (54.6% at 10 µg/mL), primarily without S9-mix, which was even more pronounced than for NM-111 at identical mass concentrations. All test items did not increase structural chromosome aberration in cultured mammalian somatic cells under the test conditions used.

Table 36: Relevant mutagenicity/transformation studies *in vitro*

Bioassay **Test system**	**Test item** **Concentration** **With/without metabolic activation (+/- S9 mix)**	**Results**	**Remarks**	**Reference**
In Vitro Bacterial Reverse Mutation Assay (Ames)	**NM-113**: 20, 100, 500, 2500 and 5000 µg/plate (-S9-mix)	negative	Precipitation about 500 µg/plate; Bateriotoxic effect about 2500 µg/plate	BASF SE (2012a)
In Vitro Bacterial Reverse Mutation Assay (Ames)	**Z-COTE MAX**: 20, 100, 500, 2500 and 5000 µg/plate (+/- S9-mix)	negative	Precipitation about 2500 µg/plate;	BASF SE (2009c)

Bioassay **Test system**	**Test item** **Concentration** **With/without metabolic activation (+/- S9 mix)**	**Results**	**Remarks**	**Reference**
In Vitro Bacterial Reverse Mutation Assay (Ames)	**NM-113**: 20, 100, 500, 2500 and 5000 µg/plate (- S9-mix)	negative	Precipitation about 500 µg/plate; Bateriotoxic effect about 2500 µg/plate	BASF SE (2012a)
In Vitro Bacterial Reverse Mutation Assay (Ames)	**Z-COTE MAX**: 20, 100, 500, 2500 and 5000 µg/plate (+/- S9-mix)	negative	Precipitation about 2500 µg/plate;	BASF SE (2009c)
In Vitro Mammalian Cell Gene Mutation Test Mouse lymphoma L5178Y/TK$^{\pm}$ cells	**NM-111**: 0, 1, 2, 4, 5, and 6 µg/mL (- S9-mix); 0, 2.5, 5, 7.5, and 10 µg/mL (+ S9-mix) **NM-110** and **NM-113**: 4 µg/mL (- S9-mix); 7.5 µg/mL (+ S9-mix)	ambiguous	Increase in mutant frequency always linked to cytotoxicity	CEFIC, Fraunhofer ITEM (2011c)
In Vitro Mammalian Chromosome Aberration Test V79 cells	**NM-111**: 0, 1, 3, 5, 10, 12.5, 15, 20, 25, and 50 µg/mL **NM-110** and **NM-113**: 0, 3, 10, and 12.5 µg/mL (4 h: +/- S9-mix; 24 h: - S9-mix)	negative	-	CEFIC, Fraunhofer ITEM (2010c)

In vivo Studies

NM-111 (purity 96-99%) was tested applying the GLP-conform Mammalian Erythrocyte Micronucleus Test according to OECD 474 (BASF, 2009b). Based on a range-finding test, 5 mice per dose group were treated once intraperitoneal (i.p.) with 15, 30, or 60 mg/kg bw of a test item suspension in fetal calf serum. The author mentioned that all animals survived at 60 mg/kg bw but distinct clinical signs were observed. More detailed information on toxicity was not indicated. 24 h (all dose groups) or 48 h (vehicle control and high dose group) after application of the test item, polychromatic erythrocytes (PCE) and normochromatic erythrocytes (NCE) from bone marrow of both femora of each animal were investigated for the presence of micronuclei. Under the experimental conditions chosen here, NM-111 did not show an increased incidence of micronuclei in bone marrow cells.

In a further Mammalian Erythrocyte Micronucleus Test (GLP-conform) according to OECD 474, five rats per dose were treated via inhalation (nose only) with 0.5, 2, and 8 mg/m^3 NM-111 (purity 98%), 8 mg/m^3 NM-110 and the reference item 8 mg/m^3 NM-113 (no details on purity) (CEFIC, 2013b). The test was conducted after 14 days of inhalation exposure (cross-reference to 0). Neither NM-111, nor NM-110 and NM-113 did significantly enhance the number of micronuclei in polychromatic erythrocytes of the bone marrow. The PCE ratio revealed no cytotoxicity.

Two further genotoxicity tests were conducted as part of 14-d Repeated Dose Inhalation Toxicity Study (CEFIC 2013b, cross-reference to 0). Male rats were exposed in the same manner as described in the 14-day Repeated Dose Inhalation Study. In a first approach, DNA-strand breaks and oxidative DNA damage (8-OH-dG) were analyzed in BAL cells of 5 males per group on day 1 and day 14 post exposure using the hOGG1-modified comet assay under non-GLP conditions. NM-111 revealed a slight dose-dependent induction of DNA-strand breaks and oxidative DNA-base lesions only after 14 days, but not on day 1 of recovery. There was statistical significance at 8 mg/m^3. A very slight significant increase in mean tail intensity was also observed for NM-113 at 8 mg/m^3, compared to the clean air control. However, this assay has to be considered as non-conclusive due to the investigative nature of the approach, the limited number of slides and especially missing consideration of viability/cytotoxicity and the cell type used (alveolar macrophages and not epithelial cells. In a second approach, formalin-fixed tissue of the terminal bronchioles and lung parenchymal cells were examined for the formation of 8-OH-dG by an antibody labeling technique. The results revealed that only the bulk ZnO (NM-113) at day 1 post exposure caused a slight but statistically non-significant increase in 8-OH-dG positive nuclei per area compared to the control group. Finally, considering the inconsistencies within and between both approaches, noconclusion can be drawn.

Table 37: Relevant mutagenicity studies *in vivo*

Study Type	Test item Dose level/ Concentration Duration	Result	Remark	Reference
In Vivo Mammalian Erythrocyte Micronucleus	**NM-111**: 0, 15, 30, or 60 mg/kg bw	negative	In the pretest distinct clinical	BASF SE (2009b)

Study Type	Test item Dose level/ Concentration Duration	Result	Remark	Reference
Test			signs were observed at 60 mg/kg bw	
In Vivo Mammalian Erythrocyte Micronucleus Test	**NM-111**: 0, 0.5, 2, and 8 mg/m^3 **NM-110**: 8 mg/m^3 **NM-113**: 8 mg/m^3	negative	Administration: nose-only inhalation, was conducted as a part of Repeated Dose Inhalation Toxicity Study	CEFIC (2013b)
hOGG1-modified comet assay	**NM-111:** 0, 0.5, 2, and 8 mg/m^3 **NM-110:** 8 mg/m^3 **NM-113:** 8 mg/m^3	Inconclusive	Administration: nose-only inhalation, was conducted as a part of Repeated Dose Inhalation Toxicity Study	CEFIC (2013b)
Immunohistochemical detection of oxidative DNA damage	**NM 111:** 0, 0.5, 2, and 8 mg/m^3 **NM 110:** 8 mg/m^3 **NM 113:** 8 mg/m^3	negative	Administration: nose-only inhalation, was conducted as a part of Repeated Dose Inhalation Toxicity Study	CEFIC (2013b)

Summary and conclusion

The results of the in vitro Bacterial Reverse Mutation Assay revealed no relevant increase in mutant frequency for NM-113 and Z-COTE MAX (based on the coated NM-111) when tested under comparable conditions.

The results of the *in vitro* Mammalian Cell Gene Mutation Test in L5178Y/TK± cells are considered as ambiguous for NM-111, NM-110 as well as for NM-113 as increases in mutant frequency were always linked to cytotoxicity.

In vitro, NM-110, NM-111, and NM-113 did not induce chromosomal aberrations in V79 cells, even at the highest cytotoxic concentration.

In vivo, NM-111 did not show an increased incidence of micronuclei in bone marrow cells in a standard test in mice.

In rats the same negative result was observed for NM-111, NM-110 and NM-113 in a Mammalian Erythrocyte Micronucleus Test following inhalation exposure.

Furthermore, no clear indication of oxidative DNA damage induced by NM-111, NM-110 and NM-113 after inhalation exposure was observed.

In conclusion, uncoated nano ZnO, coated nano ZnO and the bulk product showed the same behaviour regarding mutagenicity. No induction of gene mutations in bacteria or chromosomal aberrations *in vitro* or increased incidence of micronuclei *in vivo* or a clear indication of oxidative DNA damage were observed.

Carcinogenicity

There is no study available.

Toxicity to Reproduction

Studies in Animals

Effects on Fertility

There is no study available.

Developmental Toxicity

Inhalation

NM-111 was investigated for its prenatal developmental toxicity in Wistar rats (BASF SE, 2013) according to OECD 414 under GLP conditions. The substance was head-nose exposed to respirable dust aerosols for 6 hours per day to groups of 25 time-mated female Wistar rats at target concentrations of 0.3, 1.5, and 7.5 mg/m^3 on gestation days (GD) 6 through 19. The concurrent control group, consisting of 25 females, was exposed to conditioned air. Under the conditions of this prenatal developmental toxicity study, the inhalative administration of NM-111 at a dose of 7.5 mg/m^3 caused moderate alveolar lipoproteinosis and slight inflammation. In conclusion, the no observed adverse effect concentration (NOAEC) for maternal toxicity was1.5 mg/m^3 and the NOAEC for prenatal developmental toxicity was 7.5 mg/m^3 as the highest concentration used during the present study. There were no adverse fetal findings evident at any concentration.

Table 38: Relevant multigeneration reproduction toxicity study

Species, Strain, number, sex/group	Test item, Study type, concentrations	NOAEC, findings, remarks	Reference

Rat, Wistar, 25 pregnant females per dose	**NM-111** Prenatal Developmental Toxicity Study 0, 0.3, 1.5, and 7.5 mg/m^3	Maternal toxicity: NOAEC = 1.5 mg/m^3 (moderate alveolar lipoproteinosis and slight inflammation at 7.5 mg/m^3) Developmental toxicity: NOAEC = 7.5 mg/m^3	BASF SE (2013)

Conclusion

The NOAEC for maternal toxicity for NM-111 was determined to be 1.5 mg/m^3 and the NOAEC for developmental toxicity was 7.5 mg/m^3, the highest dose tested.

Specific Investigations

The formation of reactive oxygen species (ROS) was measured by using a lucigenin-based chemiluminescence-based assay, while the production of cytokines (IL-6, TNFα, CINC-1) and prostaglandin E2 was determined by ELISA system in rat alveolar macrophages after 24 hours exposure with ready-to-use suspensions (15 – 15000 µg/mL) of NM-111, NM-110 or NM-113 (CEFIC, 2011b). In addition, LDH release was determined to assess cell viability measured by a photometrical assay based on the conversion of a tetrazolium salt to formazan. The studies were conducted under GLP conditions. The results indicated, no ROS or cytokine production in the presence of the test items. At the highest, cytotoxic concentration, all test items increased the production of prostaglandin E2. However, no further details were provided on cytotoxicity.

Finally, with regards to the validity of these investigations, it should be considered that nanoparticle (metal oxide nanoparticle, trace metal-containing particles) may interfere with ELISA assay or LDH assay (Guidance on information requirements and chemical safety assessment, Appendix R7-1, Chapter R7a, Nanomaterials).

The study (non-guideline conform) assessed the capacity of *in vitro* screening studies to predict *in vivo* pulmonary toxicity of fine or nanoscale particles in rats. In the *in vivo* component of the study, rats were exposed by intratracheal instillation to 1 or 5 mg/kg with nano-sized zinc oxide or fine-sized ZnO (Sayes et al. 2007). Following exposure, the lungs of exposed rats were lavaged and inflammation (neutrophil recruitment) and cytotoxicity endpoints (bronchoalveolar lavage [BAL] fluid lactate dehydrogenase [LDH] values) were measured at 24 h, 1 week, 1 and 3 months post exposure. For the in vitro component, cultures of rat L2 lung epithelial cells, primary alveolar macrophages (AMs), as well as AM-L2 lung epithelial cell cocultures were incubated with the particle mentioned above. The culture fluids were evaluated for cytotoxicity endpoints (LDH, MTT) as well as inflammatory cytokines (macrophage inflammatory 2 protein [MIP-2], tumor necrosis factor alpha [TNF-alpha], and interleukin-6 [IL-6]) by using enzyme immunometric assay kits at one (i.e. cytokines) or several (cytotoxicity) time points. Results of in vivo pulmonary toxicity studies demonstrated that nano-sized and fine-sized ZnO particles produced potent but reversible inflammation which was resolved by 1 month post installation exposure. Results of in vitro pulmonary cytotoxicity studies, regarding to the LDH results, demonstrated that L2 cells the most sensitive

to nano- and fine-sized ZnO. Macrophages essentially were resistant and epithelial macrophage cocultures generally reflected the epithelial results at 4 and 24 h incubation, but not at 48 h incubation. Both ZnO particles produced very little IL-6 in macrophages and cocultures, but this effect was not dose-related. Both nanoparticles showed a similar behaviour with regard to cytotoxicity and inflammation. It should be noted that nanoparticle (metal oxide nanoparticle, trace metal-containing particles) may interfere with ELISA assay or LDH assay. This is reflected by inhibition of LDH (reduced indication of necrosis) or cytokine adsorption (reduced indication of cytokine concentration), respectively (Guidance on information requirements and chemical safety assessment, Appendix R7-1, Chapter R7a, Nanomaterials).

Microfine uncoated ZnO (Z-Cote®, corresponding to NM-110) was tested in an *in vitro* cytogenetic assay in Chinese Hamster Ovary (CHO) cells in the presence and absence of UV light to clarify whether the slightly pronounced clastogenicity *in vitro* in the dark is a genuine photo-genotoxic effect. The effect of ZnO exposure was investigated in the cells with no irradiation in the dark (D), under pre-imposed irradiation (PI, i.e. UV irradiation of cells prior to treatment with ZnO) and under simultaneous irradiation conditions (SI, i.e. ZnO treatment concurrent with UV irradiation). The cytotoxicity of ZnO to CHO cells under the different irradiation conditions was as follows: SI > PI >D. In the dark, ZnO produced a concentration-related increase in chromosome aberrations. In PI or SI CHO cells, ZnO was clastogenic at significantly lower concentrations when compared with effective concentrations in the dark. The incidence of chromosome aberrations in SI or PI cells was generally higher than that in the dark. At similar ZnO concentrations, SI conditions generally produced higher chromosome aberrations incidence than PI conditions. However, when ZnO concentrations producing similar cytotoxicity were compared, chromosome aberrations incidences under PI or SI conditions were nearly identical. The results provide evidence that minor increases in clastogenic potency under conditions of photo-genotoxicity testing do not necessarily represent a photo-genotoxic effect, but may occur due to an increased sensitivity of the test system subsequent to UV irradiation (Dufour et al., 2006).

Overall Summary and Conclusion of the Toxicological Profile

The toxicological profile of coated nanoscale ZnO (NM-111) and uncoated nanoscale ZnO (NM-110, NM-112) were investigated and compared to non-scale ZnO (NM-113).

When the nanomaterials were tested in a comparative manner, no relevant differences were noted in the toxicological profile.

In vitro and *in vivo* toxicokinetics studies were conducted to determine the dermal absorption of NM-110 and NM-111. *In vitro*, no Zn^{2+} (assumed but in the report only Zn was provided) from the NM-110 containing formulation or zinc oxide particles penetrated into or through the skin of domestic pigs. *In vivo*, NM-111 was not absorbed after dermal application in rats. Furthermore, *in vitro* and *in vivo* studies exhibited that UVB exposure of porcine skin did not enhance the penetration of 5% NM-110 and 5% NM-111 present in sunscreen formulations. Thus, neither NM-110 nor NM-111 was absorbed through the skin. Uncoated nano ZnO (NM-110) and coated nano ZnO (NM-111) shows the same behaviour and no high bioavailability has to be expected after skin contact. Exposure via inhalation indicated an increase of absolute Zn content from NM-111 in the lung after one day post exposure but not in any other body compartment. The uncoated nano ZnO (NM-110) and bulk ZnO (NM-113) a similar behaviour.

With regard to acute toxicity, the dermal LD_{50} for NM-111 was > 2000 mg/kg bw in rats. The oral LD_{50} value of nanoscaled ZnO powder (20 nm) was > 5000 mg/kg bw while the LD_{50} of 120 nm ZnO was > 2000 and < 5000 mg/kg bw in mice. The acute toxicity studies indicated that nano ZnO is comparable toxic to bulk ZnO. Especially the acute dermal toxicity results fit to skin penetration data.

NM-110 was not irritant to eye *in vitro* and NM-111 was not corrosive to skin *in vitro*. In conclusion, uncoated nano ZnO (NM-110) and coated nano ZnO (NM-111) exhibit no reactivity.

Repeated dose inhalation studies were conducted for different durations with the test item NM-111 in comparison to the reference material NM-113. Both test items caused comparable and reversible histopathological findings restricted to the respiratory tract due its particular structure. The NOAEC (NM-111) was determined to be 1.5 mg/m^3 and 2.0 mg/m^3 based on a 90-d study and 14-d study, respectively. NM-110 which was tested in a 14-d repeated dose toxicity study exerted similar effects such as NM-111 and NM-113. There are no indications, that the coated nano ZnO (NM-111) was more toxic than the uncoated nano ZnO (NM-110) or the bulk product (NM-113) with repeated dosing.

In vitro, NM-111, NM-110, and NM-113 did not induce chromosomal aberrations in V79 cells. In addition, NM-113 and Z-COTE MAX (based on NM-111) did not induce *in vitro* gene mutations in bacteria. NM-111 did not show an increased incidence of micronuclei in bone marrow cells *in vivo*. The same result was observed for NM-110 and NM-113 in a supporting *in vivo* Mammalian Erythrocyte Micronucleus Test. Uncoated nano ZnO, coated nano ZnO and the bulk product shows the same behaviour regarding mutagenicity as no induction of gene mutations in bacteria and chromosomal aberrations *in vitro* or increased incidence of micronuclei or oxidative DNA damage *in vivo* was observed.

With respect to reproductive toxicity, while the NOAEC was 1.5 mg/m^3 for maternal toxicity for NM-111, the NOAEC for prenatal/developmental toxicity was 7.5 mg/m^3, the highest concentration tested.

The Table 39 summarized the relevant and reliable studies of NM-110, NM-111, NM-112, and NM-113 for the assessment of human health.

Table 39: Relevant and reliable endpoints for the assessment of human health

Endpoint	OECD NM material	Results	Remarks	Reference
Acute toxicity				
Acute dermal toxicity	NM-110	n.d.	OECD 402	CEFIC (2010a)
	NM-111	LD_{50} > 2000 mg/kg bw		
	NM-112	n.d.		
	NM-113	n.d.		
Irritation				
In vitro skin irritation	NM-110	n.d.	OECD 431	CEFIC, 2010b

	NM-111	Non-corrosive to skin		
	NM-112	n.d.		
	NM-113	n.d.		
In vitro eye irritation	NM-110	No eye irritation potential	According to MatTek Corporation (2010) and Harbell et al. (2009)	BASF SE (2011b)
	NM-111	n.d.		
	NM-112	n.d.		
	NM-113	n.d.		
Repeated Dose Inhalation Toxicity Study				
90 d	NM-110	n.d.	OECD 413	CEFIC (2011a)
	NM-111	NOAEC: 1.5 mg/m^3		
	NM-112	n.d.		
	NM-113	Effects were comparable to NM-111		
5 d	NM-110	n.d.	OECD 412 (exposure for only 5 days)	Ma-Hock, L. et al. (2008) BASF SE (2010)
	NM-111	LOAEC: 0.5 mg/m^3		
	NM-112	n.d.		
	NM-113	Effects were comparable to NM-111		
14 d	NM-110	Effects were comparable to NM-111 and NM-113	OECD 412	CEFIC (2013b)
	NM-111	NOAEC = 2 mg/m^3		
	NM-112	n.d.		
	NM-113	Effects were comparable to NM-110 and NM-111		
5 d	NM-110	n.d.	OECD 412 (dose range finding study for CEFIC 2013b)	CEFIC (2009)
	NM-111	histopathological findings concerning nasal and paranasal activities, lungs and		

		lung-associated lymph nodes		
	NM-112	n.d.		
	NM-113	n.d.		
Mutagenicity				
In Vitro Bacterial Reverse Mutation Assay	NM-113	negative	OECD 471	BASF SE (2012a)
In Vitro Bacterial Reverse Mutation Assay	Z-COTE MAX (based on NM-111)	negative	OECD 471	BASF SE (2009c)
In Vitro Mammalian Chromosome Aberration Test	NM-110	negative	OECD 473	CEFIC, Fraunhofer ITEM (2010c)
	NM-111			
	NM-112	n.d.		
	NM-113	n.d.		
In Vitro Mammalian Cell Gene Mutation Test	NM-110	ambiguous	OECD 476	CEFIC, Fraunhofer ITEM (2011c)
	NM-111			
	NM-112	n.d.		
	NM-113	n.d		
In Vivo Mammalian Erythrocyte Micronucleus Test	NM-110	n.d.	OECD 474	BASF (2009b)
	NM-111	negative		
	NM-112	n.d.		
	NM-113	n.d.		
In Vivo Mammalian Erythrocyte Micronucleus Test	NM-110	negative	OECD 474 (administration: nose-only inhalation as a part of Repeated Dose Inhalation Toxicity Study)	CEFIC (2013b)
	NM-111			
	NM-112	n.d.		
	NM-113	negative		
Immunohistochemical detection of oxidative DNA damage	NM-110	negative	No guideline (administration: nose-only inhalation as a part of Repeated Dose Inhalation	CEFIC (2013b)
	NM-111			
	NM-112	n.d.		
	NM-113	negative		

			Toxicity Study)	
Toxicity to Reproduction				
Prenatal developmental toxicity study	NM-110	n.d.	OECD 414	BASF SE (2013)
	NM-111	Maternal toxicity: NOAEC: 1.5 mg/m^3 Developmental toxicity: NOAEC: 7.5 mg/m^3		
	NM-112	n.d.		
	NM-113	n.d.		

Finally, when comparatively tested with ZnO bulk, nanoscale ZnO revealed an almost identical bioavailability, reactivity and toxicity.

References

BASF SE (2005). Study of the penetration of zinc through dermatomed pig skin *in vitro* after treatment with a micro fine zinc oxide containing formulation (emulsion with Z-COTE (zinc oxide); 10%). Report No. 52H0546/032193, Department of Experimental Toxicology and Ecology, BASF SE, Ludwigshafen, Germany, unpublished report, 31 January 2005.

BASF SE (2009a). Flow-Through Studies on Excised UVB-Exposed Porcine Skin with BASF Formulations. Monteiro-Riviere NA and Inman A, Center for Chemical Toxicology Research and Pharmacokinetics, North Carolina State University, Raleigh, unpublished report, 16 June 2009.

BASF SE (2009b). Z-COTE HP1 Micronucleus Test in Bone Marrow Cells of the Mouse. Report-No. 26M0488/064179, BASF SE, Ludwigshafen, Germany, unpublished report, 24 August 2009.

BASF SE (2009c). Report Z-COTE MAX Salmonella Typhimurium Reverse Mutation Assay (Standard Plate Test and Preincubation Test). Report No. 40M0620/064186 (unpublished study report), testing laboratory: BASF SE, Ludwigshafen, Germany, unpublished report, 09 March 2009.

BASF SE (2010). Z-COTE HP1 Subacute 5-day lung toxicity study in male Wistar rats dust aerosol exposure. Company study no. 99I0488/06051, Department of Experimental Toxicology and Ecology, BASF SE, Ludwigshafen, Germany, unpublished report, 10 March 2010

BASF SE (2011a). Report of NM-110 Zinc Oxide Bovine Corneal Opacity and Permeability Test (BCOP Test). Company study no. 63V0656/10A319, Department of Experimental Toxicology and Ecology, BASF SE, Ludwigshafen, Germany, unpublished report, 29 July 2011.

BASF SE (2011b). Report NM-110 Zinc Oxide EpiOcular™ Eye Irritation Test. Company study no. 62V0656/10A349, Department of Experimental Toxicology and Ecology, BASF SE, Ludwigshafen, Germany, unpublished report, 21 July 2011.

BASF SE (2012a). Report of Zinc oxide nanopowder Salmonella Typhimurium Reverse Mutation Assay (Standard and Plate Preincubation Test). Report No. 40M0776/054171, testing laboratory: BASF SE, Ludwigshafen, Germany unpublished report

BASF SE (2012b). NM-110 Zinc Oxide – Determination of the Inhibition of Oxygen Consumption in the Activated Sludge Respiration Inhibition Test. Report No. 08G0656/10G095, Experimental, Toxicology and Ecology, BASF SE, Ludwigshafen, Germany, 08 November 2012.

BASF SE (2013). Report Z-COTE HP1 Prenatal Developmental Toxicity Study in Wistar rats Administration via Inhalation. Report No. 32R0488/06I005, testing laboratory: BASF SE, Experimental, Toxicology and Ecology. Owner company: CEFIC, Belgium

CEFIC (2009). 5-Day Nose-Only Inhalation Toxicity Study of Z-COTE HP1 in Wistar WU Rats (DRF Study), testing laboratory: Fraunhofer ITEM, Germany, Report No. 02N09515. Owner company: CEFIC, Brussels, Belgium

CEFIC (2010a). Acute Dermal Toxicity Test with Z-COTE HP1 in Rat – Limit Test -, testing laboratory: Fraunhofer ITEM, Germany, Report No. 02G09021. Owner Company: CEFIC, Brussels, Belgium, 30 July 2010.

CEFIC (2010b). Z-COTE HP1 *In Vitro* Skin Corrosion: Human Skin Model Test, testing laboratory: FREY TOX GmbH, Germany, Report No. 03330. Owner company: CEFIC, Brussels, Belgium, 12 May 2010.

CEFIC (2010c). In Vitro Mammalian Chromosome Aberration Test (V79 Cells) with Z-COTE HP1, testing laboratory: Fraunhofer ITEM, Report No. 17G09019. Owner company: CEFIC, Brussels, Belgium.

CEFIC (2011a). 3-Month Nose-Only Inhalation Toxicity Study of Z-COTE HP1 in Wistar WU Rats, testing laboratory: Fraunhofer ITEM, Hannover, Germany, Report No. 02G10024. Owner company: CEFIC, Brussels, Belgium.

CEFIC (2011b). Measurement of ROS formation and cytokines in rat alveolar macrophages after exposure to zinc oxide particles, testing laboratory: Fraunhofer ITEM, Germany, Report No. 18N11535. Owner company: CEFIC, 30 July 2011.

CEFIC (2011c). In Vitro Mammalian Cell Gene Mutation Test in Mouse Lymphoma L5178Y/TK Cells with Z-COTE HP1, testing laboratory: Fraunhofer ITEM, Report No. 02G09005. Owner company: CEFIC, Brussels, Belgium.

CEFIC (2013a). Dermal Absorption of [65Zn] Z-COTE HP1 in Rats, testing laboratory: Fraunhofer ITEM, Report No. 03G10027. Owner company: CEFIC, Belgium, 28 July 2011.

CEFIC (2013b). 14-day Nose-Only-Inhalation Toxicity Study of Z-COTE HP1 in Wistar WU Rats, testing laboratory: Fraunhofer ITEM, Hannover, Germany, Report No. 02G09005 (Draft Report). Owner

company: CEFIC, Brussels, Belgium. [SCC minor remark: In the meantime, there should be a final report available] Final Report available!

Cross S.E., Innes B., Roberts M.S., Tsuzuki T., Robertson T.A., McCormick P. (2007) Human Skin Penetration of Sunscreen Nanoparticles: In-vitro Assessment of a Novel Micronized Zinc Oxide Formulation. Skin Pharmacology and Physiology 20:148-154.

COLIPA AISBL (2009). Zinc Oxide – Comparative Study on the Toxicity of Nanoscale Zinc Oxides in Wistar Rats after i.v. Administration and Observation Period up to 4 Weeks, testing laboratory: BASF SE Experimental Toxicology and Ecology, Ludwigshafen, Germany, Report No. 38C0488/06106, 12 September 2009.

Commonwealth Scientific and Industrial Research Organisation (CSIRO) (2012). Retention of NM-110 in soils. Testing laboratory: Adelaide SA.

Cornelis G., Kirby J.K., Beak D., Chittleborough D., and McLaughlin M.J. (2010). A method for determination of retention of silver and cerium oxide manufactured nanoparticles in soils. Environ. Chem. 7: 298-308.

Dufour EK, Kumaravel T, Nohynek GJ, Kirkland D, Toutain H (2006) Clastogenicity, photo-clastogenicity or pseudo-photo-clastogenicity: Genotoxic effects of zinc oxide in the dark, in pre-irradiated or simultaneously irradiated Chinese hamster ovary cells, Mutation Research 607, 215–224

Escubed Ltd., 2012

European Chemicals Agency (2012). ECHA Guidance on information requirements and chemical safety assessment Appendix R7-1 Recommendations for nanomaterials applicable to Chapter R7a Endpoint specific guidance, ECHA-12-G-03-EN,

European Commission Joint Research Centre Institute for Reference Materials and Measurements (2011). NM-Series of Representative Manufactured Nanomaterials Zinc Oxide NM-110, NM-111, NM-112, NM-113 Characterisation and Test Item Preparation, JRC 64075 ISBN 978-92-79-22215-3, European Commission Joint Research Centre Institute for Reference Materials and Measurements

Fabrega J. and Galloway T.S. (2010). Interim report for ecotoxicology testing of manufacturing ZnO and CeO2 nanoparticles, testing laboratory: University of Exeter and Birmingham. Owner company: University of Exeter.

Fabrega J., Tantra R., Amer A., Stolpe B., Tomkins J., Fry T., Lead J.R., Tyler C.R, and Galloway T.S. (2010). Sequestration of Zinc from Zinc Oxide Nanoparticles and Life Cycle Effects in the Sediment Dweller Amphipod Corophium volutator. Environ. Sci. Technol.

Franklin N.M. (2007). Comparative Toxicity of Nanoparticulate ZnO, Bulk ZnO, and ZnCl2 to a Freshwater Microalga (Pseudokirchneriella subcapitata): The Importance of Particle Solubility. Environmental Science & Technology 41 (24): 8484-8490. TOXICOLOGICAL SCIENCES 118(1), 140–149

Gulson B., McCall M., Korsch M., Gomez L., Casey P., Oytam Y., Taylor A., McCulloch M., Trotter J., Kinsley L., and Greenoak G. (2010). Small Amounts of Zinc from Zinc Oxide Particles in Sunscreens Applied Outdoors Are Absorbed through Human Skin.

Gulson, Wong H, Korsch M, Gomez L, Casey P, McCall M, McCulloch M, Trotter J, Stauber J, Greenoak J (2012) Comparison of dermal absorption of zinc from different sunscreen formulations and differing UV exposure based on stable isotope tracing, Science of the Total Environment 420: 313–318

Harbell J.W. et al. (2009). COLIPA Program on Optimization of Existing In Vitro Eye Irritation Assays for Entry into Formal Validation: Technology Transfer and Intra/Inter Laboratory Evaluation of EpiOcular Assay for Chemicals. Poster # 378, SOT 2009

Heinlaan M. et al. (2008). Toxicity of nano sized and bulk ZnO, CuO and TiO2 to bacteria Vibrio fischeri and crustaceans Daphnia magna and Thamnocephalus platyurus. Chemosphere 71: 1308-1316

Landsiedel R, Schulz M, Kapp MD, Oesch F (2009). Genotoxicity Investigations on Nanomaterials: Methods, Preparation and Characterization Test Material, Potential Artifacts and Limitations – Many Questions, Some Answers. Mutation Research 681 (2-3): 241-58.

Lin D. and Xing B. (2007). Phytotoxicity of nanoparticles: Inhibition of seed germination and root growth. Environmental Pollution 150: 243-250.

Lin D. and Xing B. (2008). Root uptake and phytotoxicity of ZnO nanoparticles. Environmental Science and Technology 42: 5580-5585.

Ma-Hock, L. et al. (2008). Inhalation toxicity of nanoscale zinc oxide in comparison with pigmentary zinc oxide using short-term inhalation test protocol. Naunyn-Schmiedeberg's Arch Pharmacol (Supplement 1), 354.

MatTek Corporation, Ashland, MA 01721, USA: EpiOcularTM human cell construct: Procedure details, Version 3.1a of February 10, 2010.

Monteiro-Riviere N.A., Wiench K., Landsiedel R., Schulte S., Inman A.O., Riviere J.E. (2011). Safety Evaluation of Sunscreen Formulations Containing Titanium Dioxide and Zinc Oxide Nanoparticles in UVB Sunburned Skin: An In Vitro and In Vivo Study. Toxicological Sciences 123 (1): 264-280.

National Physical Laboratory (NPL)(2010). Interim Report on the Physico-Chemical Characterisation of PROSPEcT Nanomaterials, NPL REPORT AS 53, ISSN 1754-2928

OECD (2012). OECD Series on the Safety of Manufactured Nanomaterial No. 36 - ENV/JM/MONO(2012)40 Guidance on Sample Preparation and Dosimetry for the Safety Testing of Manufactured Nanomaterials

OECD (2014). OECD Series on the Safety of Manufactured Nanomaterial No. 41 - ENV/JM/MONO(2014)15 Report of the OECD expert meeting on the physical chemical properties of manufactured nanomaterials and test guidelines, PROSPEcT(2010), Protocol for Nanoparticle Dispersion

Osmond-McLeod M.J., Oytam Y., Kirby J.K., Gomez-Fernandez L., Baxter B., and McCall M.J. (2014) Dermal absorption and short-term biological impact in hairless mice from sunscreens containing zinc oxide nano- or larger particles. Nanotoxicology 8(S1): 72–84

Rogers N. J. et al., (2010) Physico-chemical behaviour and algal toxicity of nanoparticulate CeO2 in freshwater. Environmental Chemistry. 2010, 7, 50–60

Sanders M.B., Roberts E., Lyons B.P., and Hutchinson, T. (2012). Effects of zinc oxide nanoparticles on survival and growth of Danio rerio, testing laboratory: Cefas Weymouth, Report No. C5198. Owner company: University of Exeter.

Sayes C.M., Reed, K.L., and Warheit, D.B. (2007). Assessing Toxicity of Fine and Nanoparticles: Comparing *In Vitro* Measurements to *In Vivo* Pulmonary Toxicity Profiles. Toxicological Sciences 97 (1): 163-180.

State Office for the Environment, Measurements and Nature Conservation of the Federal State of Baden-Württemberg (LUBW) (2014). "Nanomaterialien: Charakterisierung und Messung"

The scientific committee on cosmetic products and non-food products intended for consumers (2003), opinion concerning zinc oxide SCCNFP/0649/03

Wang B, Feng W, Wang M, Wang T, Gu Y, Zhu M, Ouyang H, Shi J, Zhang F, Zhao Y, Chai Z, Wang H, Wang J (2008) Acute toxicological impact of nano- and submicro-scaled zinc oxide powder on healthy adult mice, J. Nanopart Res., 10, 263-267

Wiench et al. (2009). Acute and chronic effects of nano- and non-nanoscale TiO2 and ZnO particles on mobility and reproduction of the freshwater invertebrate Daphnia magna (undated Draft Report). Chemosphere 76 (10): 1356-1365.

Zhu X. et al. (2008). Comparative toxicity of several metal oxide nanoparticle aqueous suspensions to zebrafish (Danio rerio) early developmental stage. Journal of Environmental Science and Helath Part A 43: 278-284.

Zvyagin A. et al (2008). Imaging of zinc oxide nanoparticle penetration in human skin in vitro and in vivo. Journal of Biomedical Optics 13(6) 064031.

Annex

IUCLID Dossier Print File on Nano Zinc Oxide (CAS 1314-13-4) Sections 4, 5, 6 and 7, 20 August 2015